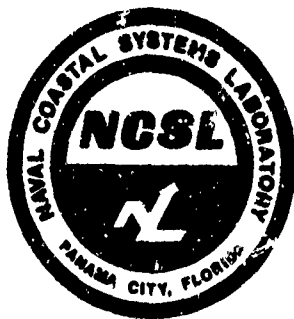


AD 745734

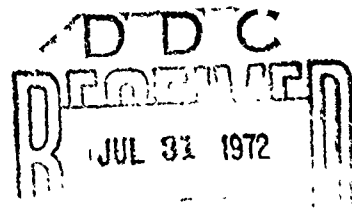


REPORT
NCSL 117-72

JUNE 1972

DESIGN, CONSTRUCTION, AND EVALUATION OF LIQUID AND SOLID ULTRASONIC LENSES

D. L. FOLDS



Approved for public release;
distribution unlimited.



NAVAL COASTAL SYSTEMS LABORATORY
PANAMA CITY, FLORIDA 32401

COPY 41

84

NAVY SECTION ☒
CODE SECTION ☐
DATE ☐
INITIALS ☐
FACILITY ☐
PROJECT ☐
SUBJECT ☐
TITLE ☐
AUTHOR ☐
DISTRIBUTION ☐
REMARKS ☐
A

NAVAL COASTAL SYSTEMS LABORATORY

ABSTRACT


The sound velocity, thermal coefficient of sound velocity, and attenuation coefficients of 20 common plastics were measured and used as a basis for the design of several lenses. Materials selected were polyethylene, nylon, polystyrene, polyphenylene oxide, and a low sound velocity silicone rubber compound. Using common geometrical optical techniques, lenses were designed to minimize off-axis aberrations for focal-length-to-aperture ratios ranging from one to three and aperture to wavelength ratios up to 150. Using methods analogous to chromatic aberration correction in optics, lenses were designed for constant focal length over a temperature range of 0 to 30°C. Two- and four-element lens systems with apertures up to 30 cm were fabricated from the selected materials. Measurements were made in the frequency range 600 kHz to 1.2 MHz and good agreement with theoretical predictions of focal length and directional response was observed. The effects of shear waves were not evident. The theoretical model used to evaluate lens performance was based on the numerical evaluation of the Fresnel-Kirchoff diffraction integral. This work shows that it is possible, using established optical design methods and commonly available solid materials, to fabricate athermal acoustic lenses with good performance characteristics at aperture-to-wavelength ratios up to 150.

ADMINISTRATIVE INFORMATION

This work was performed during FY 1971 under Subproject ZF XX 112 001, Task 00112, Work Unit 21, *Development of Acoustic Lenses and Imaging Techniques for High Resolution Sonar*. This work is continuing during FY 1972 under Subproject ZF XX 112 001, Task 00401, Work Unit 42, *Development of Acoustic Imaging Techniques for High Resolution Sonar*.

The author wishes to acknowledge the support of Mr. W. Biegler, Code P751, and Mr. R. Cook, Code P722, during the mechanical design and testing phases of this work.


CAPT L O G WHALEY, USN
Commanding Officer


GERALD G GOULD
Technical Director

UNCLASSIFIED

Security Classification

DOCUMENT CONTROL DATA - R & D		
(Security classification of title, body of abstract and indexing annotation must be entered when the overall report is classified)		
1. ORIGINATING ACTIVITY (Corporate author) Naval Coastal Systems Laboratory Panama City, Florida 32401		2a. REPORT SECURITY CLASSIFICATION UNCLASSIFIED
		2b. GROUP -----
3. REPORT TITLE "DESIGN, CONSTRUCTION, AND EVALUATION OF LIQUID AND SOLID ULTRASONIC LENSES".		
4. DESCRIPTIVE NOTES (Type of report and inclusive dates) Formal Report		
5. AUTHOR(S) (First name, middle initial, last name) D. L. Folds		
6. REPORT DATE June 1972	7a. TOTAL NO. OF PAGES 83	7b. NO. OF REFS 11
8a. CONTRACT OR GRANT NO. b. PROJECT NO ZFXXX112001 c. d.		9a. ORIGINATOR'S REPORT NUMBER(S) NCSL 117-72 9b. OTHER REPORT NO(S) (Any other numbers that may be assigned this report)
10. DISTRIBUTION STATEMENT Approved for Public Release; distribution unlimited		
11. SUPPLEMENTARY NOTES		12. SPONSORING MILITARY ACTIVITY Chief of Naval Material
13. ABSTRACT The sound velocity, thermal coefficient of sound velocity, and attenuation coefficients of 20 common plastics were measured and used as a basis for the design of several lenses. Materials selected were polyethylene, nylon, polystyrene, polyphenylene oxide, and a low sound velocity silicone rubber compound. Using common geometrical optical techniques, lenses were designed to minimize off-axis aberrations for focal-length-to-aperture ratios ranging from one to three and aperture to wavelength ratios up to 150. Using methods analogous to chromatic aberration correction in optics, lenses were designed for constant focal length over a temperature range of 0 to 30°C. Two- and four-element lens systems with apertures up to 30 cm were fabricated from the selected materials. Measurements were made in the frequency range 600 kHz to 1.2 MHz, and good agreement with theoretical predictions of focal length and directional response was observed. The effects of shear waves were not evident. The theoretical model used to evaluate lens performance was based on the numerical evaluation of the Fresnel-Kirchoff diffraction integral. This work shows that it is possible, using established optical design methods and commonly available solid materials, to fabricate athermal acoustic lenses with good performance characteristics at aperture-to-wave length ratios up to 150.		

DD FORM 1 NOV 62 1473

UNCLASSIFIED

Security Classification

I

UNCLASSIFIED

Security Classification

14	KEY WORDS	LINK A		LINK B		LINK C	
		ROLE	WT	ROLE	WT	ROLE	WT
	Acoustic lens Ultrasonics High resolution sonar Construction Materials Imaging Optical Equipment Plastics Coefficients Attenuation Identifiers Thermal Coefficient of Sound Velocity Ultrasonic lenses Solid Acoustic lens Liquid filled acoustic lens						

UNCLASSIFIED

Security Classification

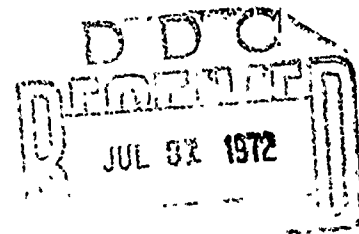


TABLE OF CONTENTS

	<u>Page No.</u>
INTRODUCTION.	1
ACOUSTIC LENS DESIGN THEORY	2
General Considerations	2
Lens Design Methods.	2
Material Properties.	3
LENS DESIGN	4
Single Refracting Surface Lens	4
Description	4
Thermal Effects	4
Depth of Focus.	7
Thin Lens in Water	10
Description	10
Aberrations	10
Thermal Aberration Analysis	14
Off-Axis Imagery.	18
Image Surface Curvature	21
Typical Designs	21
Theoretical Directional Response.	21

TABLE OF CONTENTS (CONT'D)

	<u>Page No.</u>
Thin Lens in Nonaqueous Medium	21
Lens Description.	21
Thermal Aberration Correction	23
Typical Design.	25
Aperture Blocking	28
Doublet Thin Lens.	28
Description	28
Thermal Aberration Correction	29
Coma and Spherical Aberration Correction.	31
Construction Materials.	32
Typical Designs	33
TEST RESULTS.	34
Test Facility and Procedure.	34
Test Objectives.	35
Test Results for Singlet Lenses.	35
Nylon Lens.	35
Bi-Concave Polyethylene Lenses.	41
Plano-Concave Polyethylene Lens	45
Polystyrene Lens.	46
Test Results for Doublets.	49
Polyethylene-Silicone Rubber Doublet Lens	53
Nylon-Silicone Rubber Doublet Lens.	53

TABLE OF CONTENTS (CONT'D)

	<u>Page No.</u>
Polyphenylene Oxide-Silicone Rubber Doublet Lens. .	53
Test Results for Multi-Element Lens System	58
DISCUSSION OF TEST RESULTS.	58
CONCLUSIONS	61
REFERENCES.	64
APPENDIX A - LENS CONSTRUCTION MATERIALS.	A-1
APPENDIX B - NUMERICAL CALCULATION OF PRESSURE DISTRIBUTION IN IMAGE SPACE.	B-1

LIST OF ILLUSTRATIONS

<u>Figure No.</u>		<u>Page No.</u>
1	Diagram of Single Refracting Surface Lens	5
2	Normalized Focal Length as a Function of Refractive Index	6
3	Normalized Rate of Change of Focal Length per Degree Centigrade as a Function of Refractive Index	8
4	Geometry for Axial Response Calculations	8
5	Temperature Range as a Function of Diameter-to-Wavelength Ratio and Refractive Index	11
6	Directional Response Versus Temperature for Single Refracting Surface Lens	12
7	Geometry of Thin Lens in Water	13
8	Relative Spherical Aberration Minima as a Function of Refractive Index	15
9	Relative Spherical and Comatic Aberrations as a Function of Shape Factor	16
10	Normalized Rate of Change of Focal Length as a Function of Refractive Index and Thermal Coefficient of Sound Velocity	17
11	Maximum Blur Spot Diameter as a Function of Off-Axis Angle and f/Number	19
12	Theoretical Directional Response for Nylon Thin Lens at 0°C, 20°C, and 30°C for On-Axis and 15° Off-Axis	21
13	Geometry of Thin Lens in Nonaqueous Medium	23
14	Geometry of Lens Design with Neutral Element	26
15	Dimensions of Neutral Element to Prevent Aperture Blocking	27

LIST OF ILLUSTRATIONS (CONT'D)

<u>Figure No.</u>		<u>Page No.</u>
16	Geometry of Doublet Thin Lens	29
17	Experimental Measurement Geometry	34
18	Nylon Lens Parameters	36
19	Theoretical Axial Amplitude Response	37
20	Measured On-Axis Directional Response as a Function of Axial Position (Nylon Lens)	38
21	Theoretical and Measured On-Axis Directional Response at 600 kHz (Nylon Lens)	39
22	Theoretical and Measured Directional Response at 600 kHz (Nylon Lens, 15° Off-Axis)	40
23	Theoretical and Measured Directional Response at 1052 kHz (Nylon Lens)	42
24	Polyethylene Bi-Concave Lens Parameters	43
25	Theoretical and Measured On-Axis Directional Response at 600 kHz for Three Axial Positions (Polyethylene Lens)	44
26	Theoretical and Measured On-Axis Directional Response at 1.2 MHz (Bi-Concave Polyethylene Lens)	45
27	Polyethylene Plano-Concave Lens Parameters	46
28	Theoretical and Measured On-Axis Directional Response at 600 kHz (Plano-Concave Polyethylene Lens)	47
29	Measured Directional Response at 600 kHz (Plano-Concave Polyethylene Lens, 15° Off-Axis)	48
30	Polystyrene Lens Parameters	49

LIST OF ILLUSTRATIONS (CONT'D)

<u>Figure No.</u>		<u>Page No.</u>
31	Measured On-Axis Directional Response at 600 kHz as a Function of Axial Position (Polystyrene Lens)	50
32	Theoretical and Measured On-Axis Directional Response at 600 kHz (Polystyrene Lens)	51
33	Measured Directional Response at 600 kHz (Polystyrene Lens, 20° Off-Axis)	52
34	Theoretical and Measured On-Axis Directional Response at 1 MHz (Polystyrene Lens)	52
35	Polyethylene and Silicone Rubber Doublet Lens Parameters	53
36	Theoretical and Measured On-Axis Directional Response at 600 kHz (Polyethylene/Silicone Rubber Lens)	54
37	Nylon and Silicone Rubber Doublet Lens Parameters	55
38	Theoretical and Measured On-Axis Directional Response at 600 kHz (Nylon/Silicone Rubber Lens)	56
39	Polyphenylene Oxide and Silicone Rubber Doublet Lens Parameters	57
40	Theoretical and Measured On-Axis Directional Response at 600 kHz (Polyphenylene Oxide/Silicone Rubber Lens)	59
41	Measured Directional Response at 600 kHz (Polyphenylene Oxide/Silicone Rubber Lens, 20° Off-Axis)	60
42	Multi-Element Lens Parameters	61
43	Theoretical and Measured On-Axis Directional Response at 600 kHz (Multi-Element Lens)	62

INTRODUCTION

For the past several years, considerable effort has been devoted to the development of the liquid-filled single element acoustic lens. This lens, possessing only a single refracting surface, has been investigated in both its spherical and cylindrical forms (References 1 and 2, and 3 and 4, respectively). Simple in concept, design, and construction, and offering tremendous advantages in beamforming, this lens is limited in two respects: first, the beamwidth is limited by spherical aberration to approximately 0.5 degrees, and second, the focal length is dependent upon temperature. For many applications, these limitations are not considered severe and the lenses are being employed in several experimental sonar systems.

In an effort to determine if limitations could be overcome while preserving wide field of view characteristics, a two-component concentric cylinder lens was investigated (Reference 5). This lens design corrects spherical aberration but does not correct the focal length dependence on temperature. The lens is capable of forming beams of less than 0.1 degree over a 120-degree field of view, but only under nearly constant thermal conditions. At this time a practical lens does not exist which is capable of temperature-independent diffraction-limited performance over wide fields of view at high lens diameter-to-wavelength ratios (D/λ).

To meet this goal will require multi-element lens systems analogous to high quality optical systems. In the past, little effort has been directed toward the development of multi-element lens systems, and almost no data are available concerning material parameters required for lens design. For this reason parallel investigative efforts were conducted in acoustic lens design theory and measurement of acoustic properties of materials. During this investigation, several lenses were designed, constructed, and tested to determine experimentally the feasibility of singlet and doublet lenses using solid materials.

ACOUSTIC LENS DESIGN THEORY

GENERAL CONSIDERATIONS

For a high resolution sonar beamforming application, certain constraints are often imposed by the sonar system designer. Since a heavy penalty in terms of hydrodynamic drag results when large sonar apertures are employed, it is imperative that the maximum angular resolution be realized from the aperture size available. This constraint restricts the use of aperture stops or diaphragms which are widely used in optical systems to control aberrations through a reduction in effective aperture size. For this reason, in the lens designs considered here aperture stops were not employed. Long focal length lenses are often used to control aberrations. Unfortunately, size and weight will most often restrict focal length to no more than three times the lens diameter; i.e., $f/3$ lenses. Lenses of higher f /number were not considered in this investigation.

Another constraint often imposed by the designer is that the lens must deliver nearly diffraction-limited performance over a wide field of view (60 to 120 degrees). This is a difficult design goal, particularly at high resolutions. The requirement for diffraction-limited lenses is not often observed in optical lens design, while for sonar applications the requirement is definitely justified. The angular resolution of any aperture is limited by its D/λ ratio; i.e., $\theta \approx \lambda/D$ radians. In optics, the D/λ ratio for a 5-cm lens in visible light is 1×10^6 and the spot size for an $f/2$ lens is 10^{-4} cm. Conventional film is only capable of linear resolutions in the order of 5×10^{-3} cm; hence, the lens diffraction pattern may be greatly deteriorated by aberrations with little significant image degradation. In contrast, a diffraction-limited 50 cm $f/2$ acoustic lens operating at 200 kHz has a spot size of approximately two wavelengths. Sonar transducer elements of less than 0.5 wavelengths are easily constructed and capable of resolving the lens diffraction pattern. Hence, the ultimate resolution of optical systems may be sensor limited while for sonar systems using acoustic lenses, the ultimate resolution limit will be determined primarily by the lens design. Therefore, aside from fundamental diffraction limitations present in any beamforming system, improvements in sonar system beamforming will result from designing aberration-free lens systems.

LENS DESIGN METHODS

The design of lenses is a complex procedure which can only be accomplished (with any degree of efficiency) by numerical techniques carried out by a large computer. Several optical lens design computer programs are available which, when monitored by experienced designers, are capable

of designing highly sophisticated multi-element lens systems. It has been shown that these programs can be used with no modification to design acoustic lenses. These highly developed techniques were not employed for the following reasons: first, an experienced lens designer was not available to monitor the programs; second, it was believed that more insight into the effects of the various material parameters could be gained if simple thin lens techniques were applied. Applying thin lens formulae permits one to observe the limitations imposed by available materials and limitations imposed by the degrees of freedom available in one, two, and three element lens systems.

MATERIAL PROPERTIES

The material properties of interest to the lens designer are index of refraction (n), and the rate of change of index with respect to temperature (dn/dt). The acoustic index of refraction of a given material is defined by $n = C/V$ where C is the sound velocity of the reference medium (seawater) and V is the sound velocity in the material. The parameter C is a function of temperature, pressure, and salinity, and V is a function of temperature, pressure, and frequency. During this investigation, pressure was taken to be atmospheric, temperature was confined to the range 0 to 30°C, and salinity to 0 to 35 ppm. For the materials of interest in lens design, primarily low attenuation liquids and solids, the velocity dispersion with frequency is not significant.

For most materials, velocity is a linear function of temperature and can be expressed by

$$V = V_0 + \lambda t$$

where V_0 is the velocity at 0°C and λ is the thermal coefficient of sound velocity. For solids, λ is in the range -1 to -9 and for liquids in the range -1 to -5 m/sec-°C. Water is unique in that λ is positive of magnitude near 4 m/sec-°C. The sound velocity in liquids ranges from near 450 m/sec to 2000 m/sec. Solid materials of interest have sound velocities in the range 850 to 3000 m/sec.

For almost all liquids at frequencies less than 1 MHz, attenuation is not significantly greater than for seawater. Solids are characterized when a few exceptions by high attenuation values increasing linearly with frequency.

Rigid plastics and rubbers are the most common materials examined for use in solid lens construction. This is due in large part to their low acoustic impedance (density-sound velocity product). Using these materials it is possible to achieve near matches in impedance with seawater.

Appendix A contains measured data for a large number of materials considered for lens design.

LENS DESIGN

SINGLE REFRACTING SURFACE LENS

Description

This type lens consists of a single refracting medium (liquid or solid) with an index of refraction greater than 1. In the case of a liquid medium, a thin plastic shell is used to enclose the liquid and to form the lens shape. Solid refractive media are seldom used due to the high insertion losses. The most common refracting surface shape is spherical. A cross-sectional view of a liquid lens with transducers at its spherical image surface is shown in Figure 1. Owing to its spherical symmetry, the primary advantage of this lens is a wide field of view. Lenses of this type have been constructed with an angular field of view of 120 degrees.

Thermal Effects

Although considerable research has been completed concerning the properties of the spherical lens, the analysis of thermal aberrations as presented in this section have not been reported previously.

The lens equation for a single surface is

$$\frac{n}{S} + \frac{n'}{S'} = \frac{n' - n}{r} \quad (1)$$

where S and S' are the object and image distances measured from the vertex, r is the radius of curvature, and n and n' are the indices of refraction in object and image space.

Imposing the condition $S \rightarrow \infty$ which is analogous to the far-field condition, then Equation (1) may be written as

$$f' = r \cdot n' / (n' - n) \quad (2)$$

where $S' \rightarrow f'$ is the lens focal length.

Figure 2 is a graph of focal length (in units of lens diameter D) as a function of refractive index n' . The refractive index n of the medium surrounding the lens is taken to be 1.

(Text Continued on Page 7)

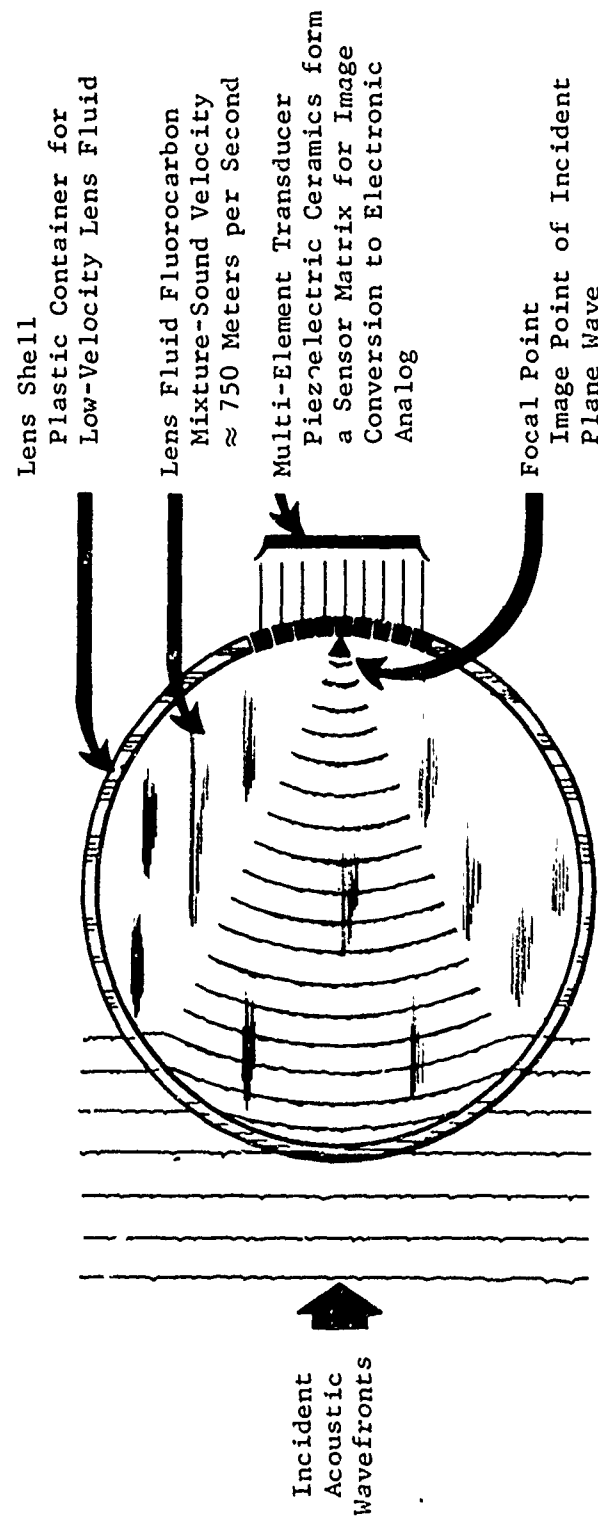


FIGURE 1. DIAGRAM OF SINGLE REFRACTING SURFACE LENS

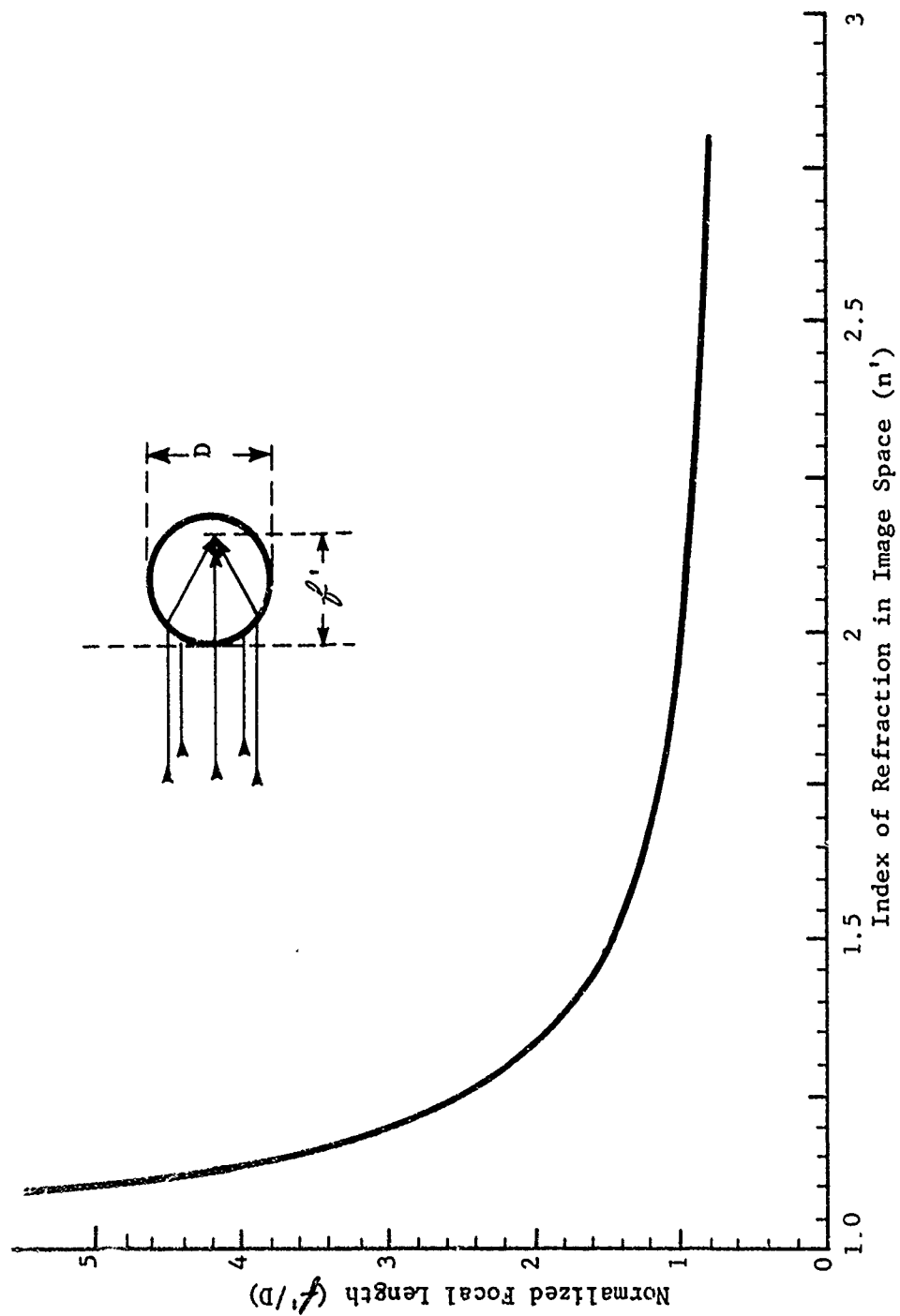


FIGURE 2. NORMALIZED FOCAL LENGTH AS A FUNCTION OF REFRACTIVE INDEX

Since n' is a function of temperature and the dependence is approximately linear, the relationship may be expressed as

$$n' = n'_0 + b't$$

where n'_0 is the index of refraction at 0°C , b' is the rate of change of index with respect to temperature, and t represents temperature. Differentiating the focal length relationship in Equation (2), it is found that

$$df'/dt = -rb'/(n' - 1)^2. \quad (3)$$

According to the physical laws governing sound velocity (V) and thermal coefficient of sound velocity (λ), the parameters n' and b' are not independent. Since $C = C_0 + 4t$ for seawater and $V = V_0 + \lambda t$ for lens liquids where $\lambda \approx -3 \text{ m/sec-}^\circ\text{C}$, then

$$b' = dn'/dt \approx n'_0(4 + 3n'_0)/C_0.$$

Using the above relationship, Equation (3) may be rewritten as

$$\frac{df'}{dt} = -f' (3n'_0 + 4)/C_0 [(n'_0 - 1) + t (6n'^2_0 + 5n'_0 - 4)] \quad (4)$$

The expression above is plotted in Figure 3 where df'/dt is plotted in units of f' using n'_0 as the independent parameter. In this figure C_0 is taken as 1442 m/sec .

These results demonstrate the amount focal length changes with a temperature change, but they do not show the seriousness of this focal shift in terms of degradation of the directional response. The degree of degradation can only be evaluated if the depth of focus is known.

Depth of Focus

For the geometry of Figure 4, it has been shown in Reference 6 that the axial intensity distribution is given by

$$I = \frac{k^2 W^4}{4R_0^4} \left[\frac{1}{1 + x/R_0} \right]^2 \left[\frac{\sin(\pi g x)}{\pi g x} \right]^2, \quad (5)$$

where

$g = n_i W^2 / [2\lambda R_0 (R_0 + x)]$, k is the wave number in image space, n_i is the refractive index in image space and W is the lens radius. Redefined in terms of the single refractive index lens, Equation (5) becomes

$$A \approx 2\pi g \sin(\pi g x) / \pi g x$$

(Text Continued on Page 9)

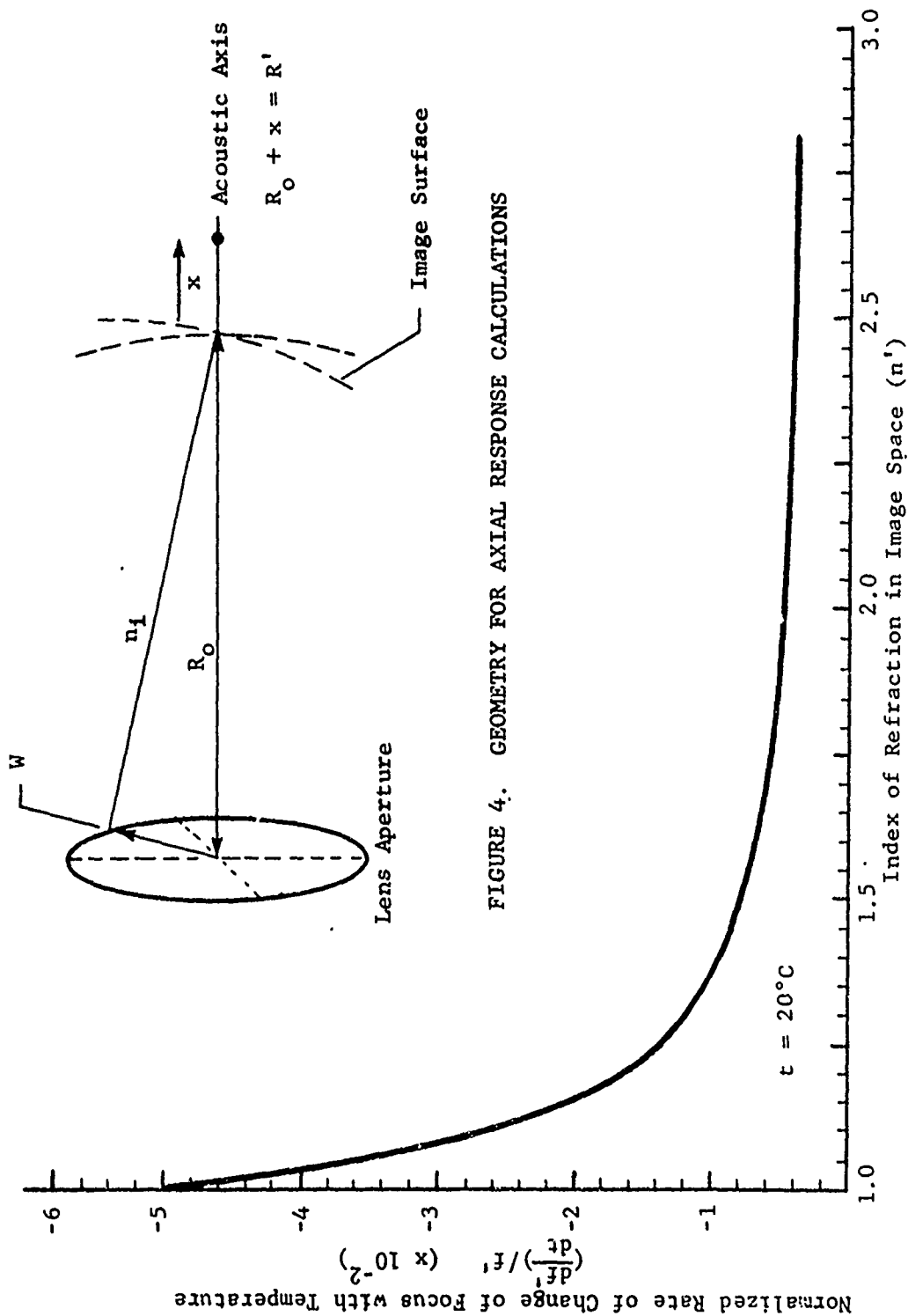


FIGURE 3. NORMALIZED RATE OF CHANGE OF FOCAL LENGTH PER DEGREE CENTIGRADE
AS A FUNCTION OF REFRACTIVE INDEX

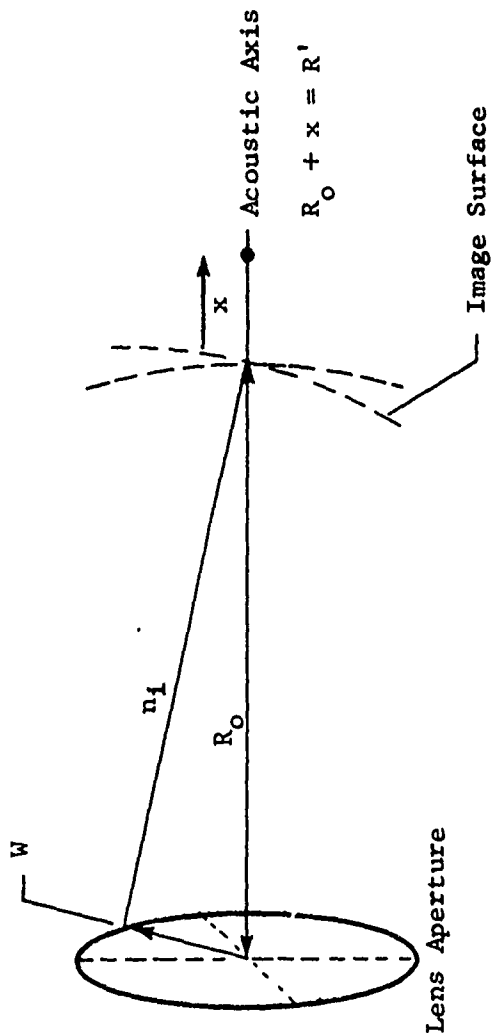


FIGURE 4. GEOMETRY FOR AXIAL RESPONSE CALCULATIONS

where A is the pressure amplitude response and

$$g = (n_1 D / \lambda) / [8 F_N (x + f')] .$$

F_N is the lens f/number defined as R_0/D , and D is the lens diameter.

To express the axial response in relative decibels (A_R) using the in-focus amplitude as the reference level, then

$$A_R = 20 \log |2 \sin(\pi g x) / (\pi g x)| / \lim_{x \rightarrow 0} [2 \sin(\pi g x) / (\pi g x)] .$$

Recognizing that the denominator is equal to 2, then

$$A_R = 20 \log |\sin(\pi g x) / (\pi g x)| . \quad (5.1)$$

The condition that image sharpness exists (a well-defined diffraction pattern) is that A_R remain at a level greater than 0.5 db below the response at the correct focal position. Stated mathematically,

$$-0.94 < \sin(\pi g x) / \pi g x < 0.94 .$$

These extreme conditions are satisfied for

$$g x = \pm 0.19 .$$

The extreme x values can now be written, using the definition of g, as

$$x^+ = \left[1.5 F_N f' / (n_1 D / \lambda) \right] \cdot \left[1 / (1 - 1.5 F_N / (n_1 D / \lambda)) \right]$$

$$x^- = - \left[1.5 F_N f' / (n_1 D / \lambda) \right] \cdot \left[1 / (1 + 1.5 F_N / (n_1 D / \lambda)) \right] .$$

For small $F_N / (D / \lambda)$ ratios, a total focal range $\Delta F = x^+ - x^-$ may be written as

$$\Delta F = 3 F_N f' / (n_1 \cdot D / \lambda) . \quad (6)$$

This result is valid for all lens types and is not restricted to the single refractive lens discussed here. The above equation will also be used in later sections dealing with other lens types.

If Equations (4) and (6) are considered, then the total temperature range over which good focusing will be maintained can be determined.

Based on the relationship $\Delta F \approx (df/dt)\Delta T$, then

$$\Delta T = [3 F_N / (n_1 D / \lambda)] \cdot [C_0(n_0' - 1) + t(6n_0'^2 + 5n_0' - 4)] / (3n_0' + 4)$$

Therefore, if the lens is optimally focused, a temperature variation

$$\Delta T = \pm [1.5 F_N / n_1 D / \lambda] \cdot [C_0(n_0' - 1) + t(6n_0'^2 + 5n_0' - 4)] / (3n_0' + 4) \quad (7)$$

could be tolerated before refocusing is required.

To further simplify this relationship, Equation (2) may be used to express F_N as $n'/2(n' - 1)$ so Equation (7) is rewritten

$$T = \pm 0.75[t + C_0 / (3n_0' + 4)] / (D / \lambda) \quad (8)$$

Figure 5 is a plot of this relationship expressing the product $T'D/\lambda$ as a function of n_0' .

To demonstrate the effects of temperature variations on directional response, the theoretical responses at four temperatures are shown in Figure 6. The computational techniques described in Reference 2 were used to obtain these plots. The lens described is spherical with $F_N = 0.7$, $D/\lambda = 35$, $n_0' = 2.2$ and $n_{20}' = 2.53$.

THIN LENS IN WATER

Description

The simple thin lens shown in Figure 7 gives an additional degree of freedom for design in the form of the radius of curvature of the second surface. Lens thickness is not a completely independent parameter since it is constrained by the radii of curvature, r_1 and r_2 . In addition, it is desirable to keep lens thickness at a minimum to reduce sound absorption losses and weight.

Thermal aberrations (change in focal length with temperature) cannot be corrected with this lens but the additional degree of freedom does permit a reduction in spherical aberrations.

Aberrations

Reference 7 gives L_S and C_S as a measure of spherical aberration and coma respectively, where

$$L_S \propto (1/[8n'(n'-1)]) \cdot [q^2(n'+2)/(n'-1) + 4(n'+1)p \cdot q + (3n' + 2)(n'-1)p^2 + n'^3/(n'-1)] \quad (9)$$

(Text Continued on Page 13)

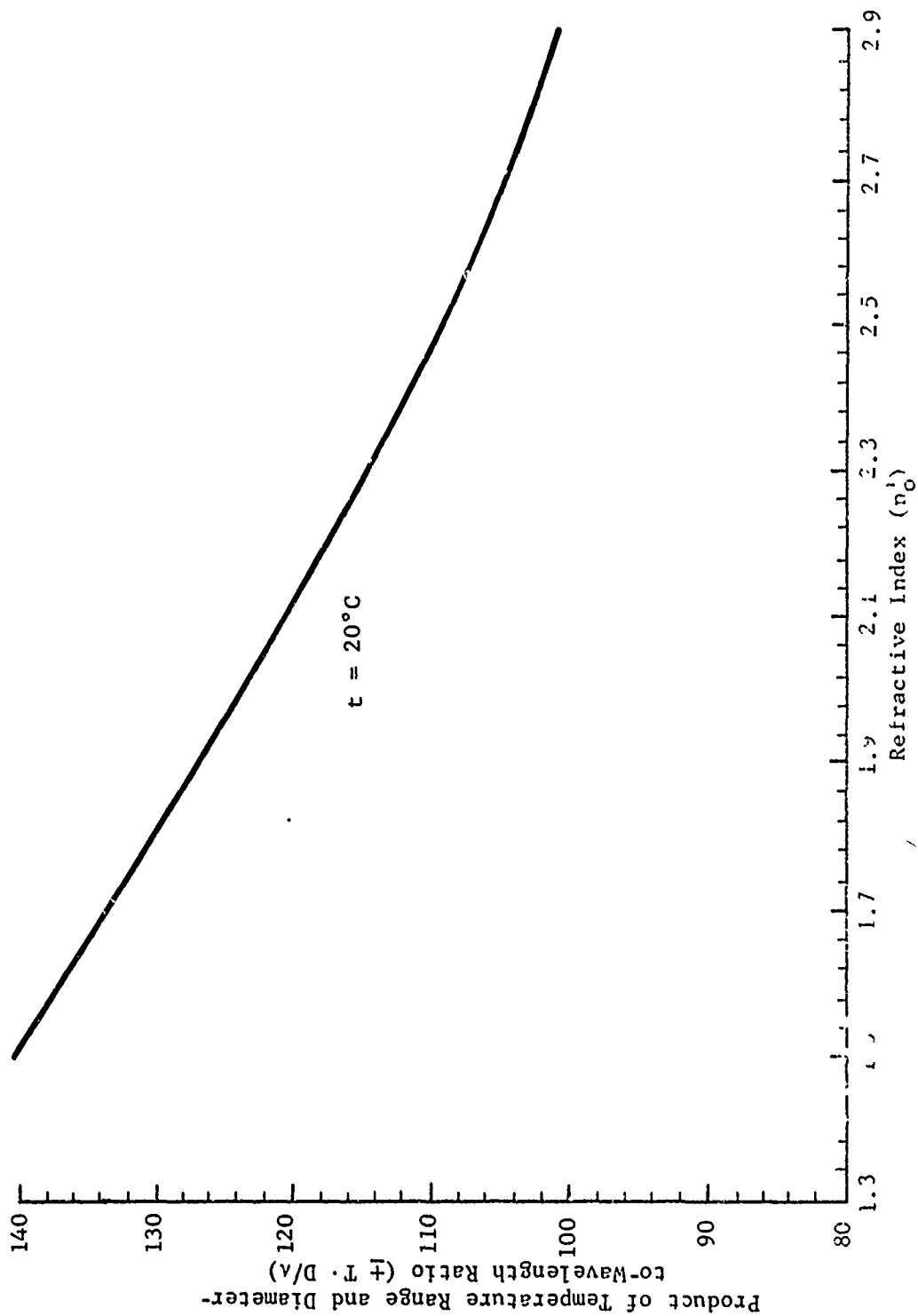


FIGURE 5. TEMPERATURE RANGE AS A FUNCTION OF DIAMETER-TO-WAVELENGTH RATIO AND REFRACTIVE INDEX

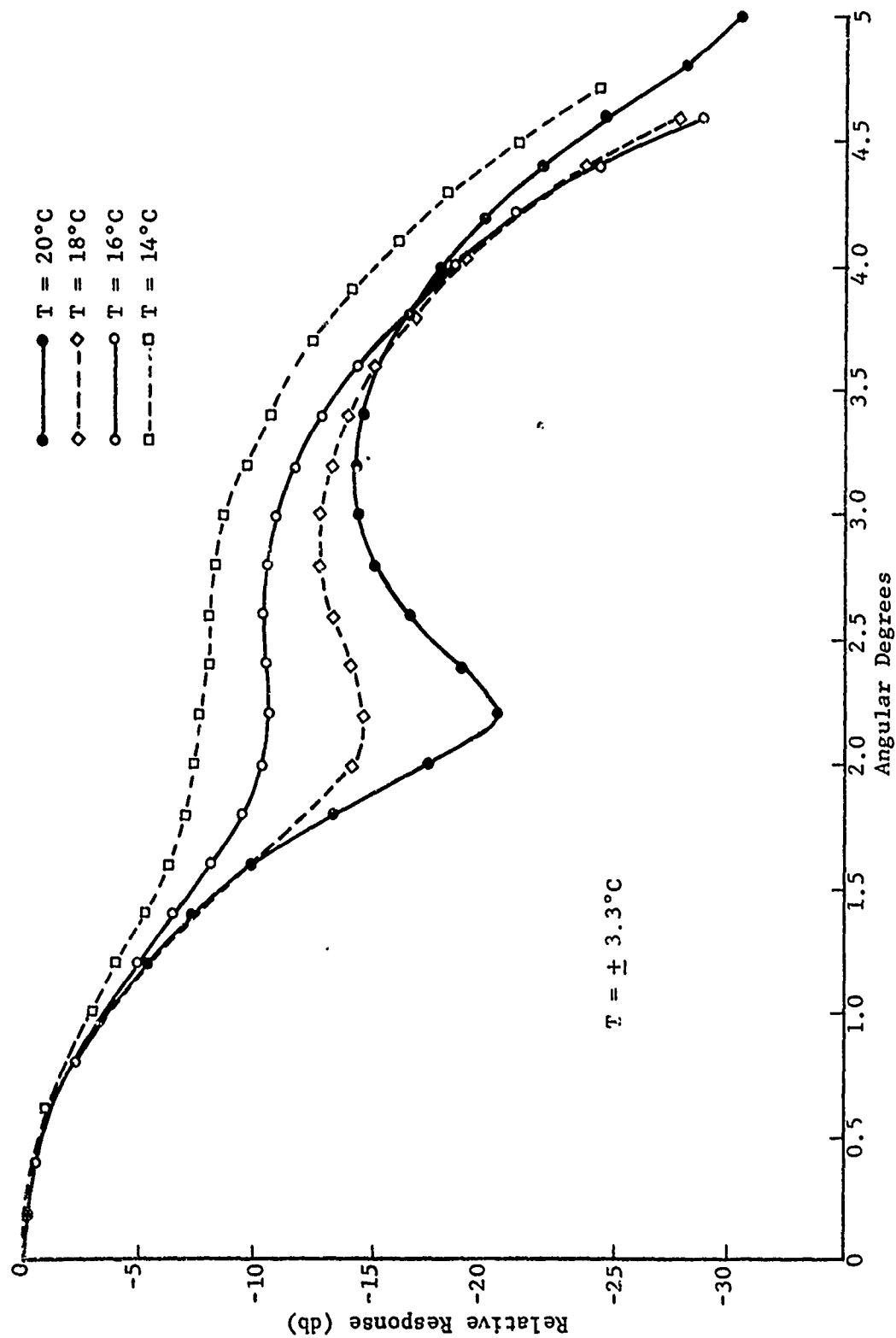


FIGURE 6. DIRECTIONAL RESPONSE VERSUS TEMPERATURE
FOR SINGLE REFRACTING SURFACE LENS

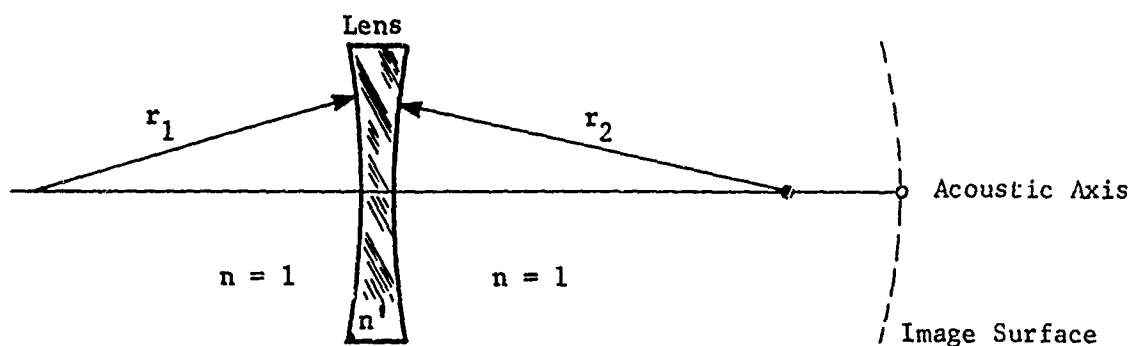


FIGURE 7. GEOMETRY OF THIN LENS IN WATER

$$C_S \propto 3p(2n' + 1)/(4n') + 3q(n'+1)/(4n'^2 - 4n') \quad (10)$$

where

$$p = (S' - S)/(S' + S) \quad (11)$$

and

$$q = (r_2 + r_1)/(r_2 - r_1) \quad (12)$$

In these expressions, p is defined as position factor and q as the lens shape factor. By differentiating L_S with respect to q , it is found that spherical aberration is minimized when

$$q = -2(n'^2 - 1) \cdot p/(n'+2). \quad (13)$$

Similarly for minimum coma,

$$q = -(2n' + 1) \cdot (n' - 1) \cdot p/(n' + 1). \quad (14)$$

Algebraic manipulation of Equation (12) and the lens equation

$$\frac{1}{f} = (n' - 1) \left(\frac{1}{r_1} - \frac{1}{r_2} \right),$$

yields the following results:

$$\begin{aligned} r_1 &= 2f(n' - 1)/(q + 1) \\ r_2 &= 2f(n' - 1)/(q - 1). \end{aligned} \quad (15)$$

Figure 8 is a plot of L_S as a function of index of refraction using the value q given by Equation (13), and an object distance of infinity ($p = -1$). This figure shows the relative minima in spherical aberration for the range of refractive indices available.

Although spherical aberration and coma cannot be minimized simultaneously, it is possible to choose a value of q which yields a good compromise in their respective values. In Figure 9 this point is illustrated by plotting relative values of L_S and C_S for $n = 0.56$, $p = -1$ as a function of q . Referring to the figure, observe that a value of $q = -0.6$ would be a good compromise between these aberration magnitudes.

Thermal Aberration Analysis

Thermal aberration cannot be corrected by this type lens but it is possible to reduce it to an acceptable value in most cases by proper choice of materials.

From the lens equation, it is found that

$$\frac{df}{dt} = -b'f/(n' - 1)$$

where

$$b' = dn'/dt = (4n'_0 - \epsilon n'^2_0)/C_0$$

or

$$df/dt = -n'_0 f (4 - \epsilon n'_0) / (C_0 \cdot (n' - 1)).$$

Figure 10 is a plot of $(df/dt)/f$ as a function of n' using ϵ as a parameter to generate a family of curves. For practical materials having good acoustic properties, the value of df/dt will be given by

(Text Continued on Page 18)

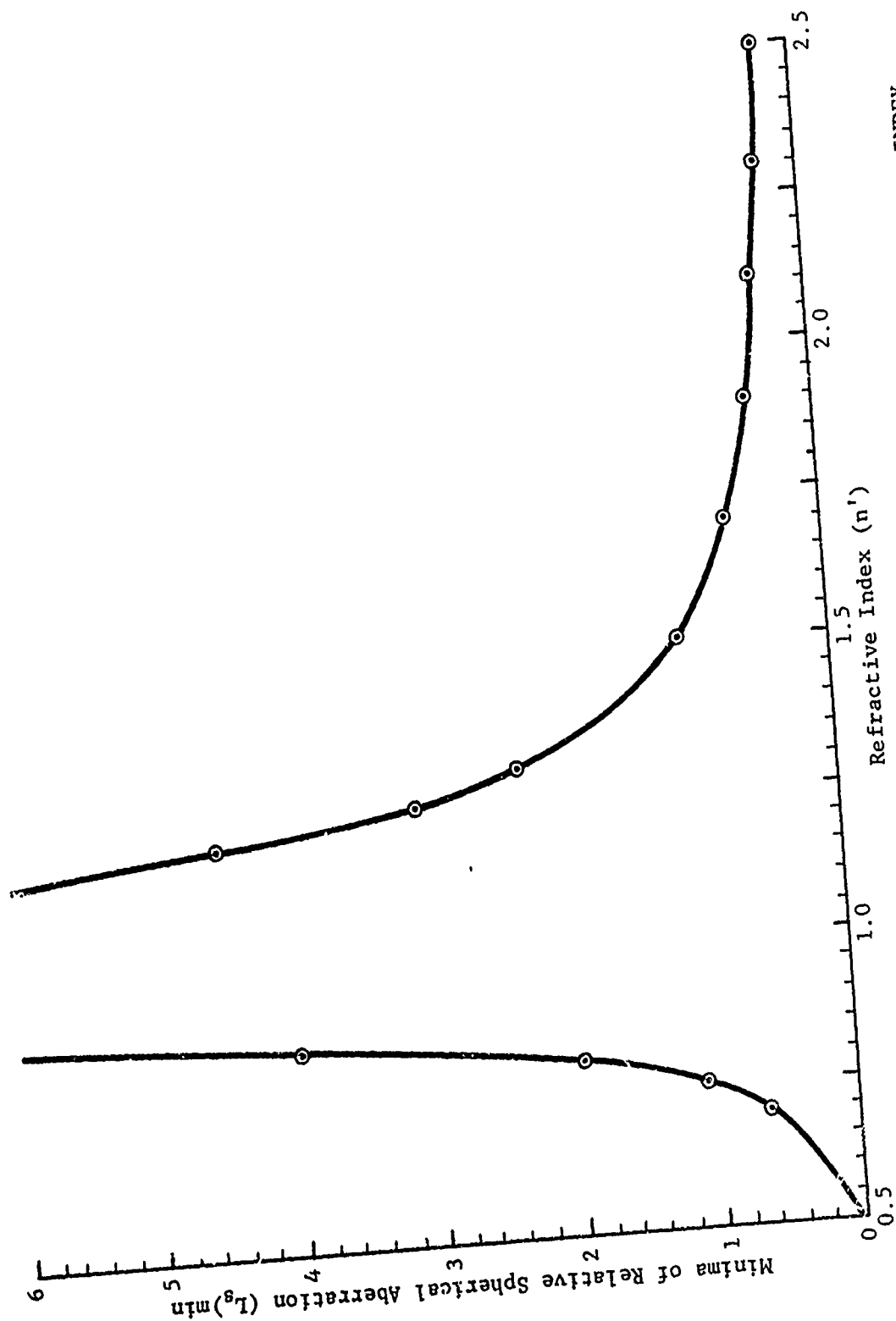


FIGURE 8. RELATIVE SPHERICAL ABERRATION MINIMA AS A FUNCTION OF REFRACTIVE INDEX

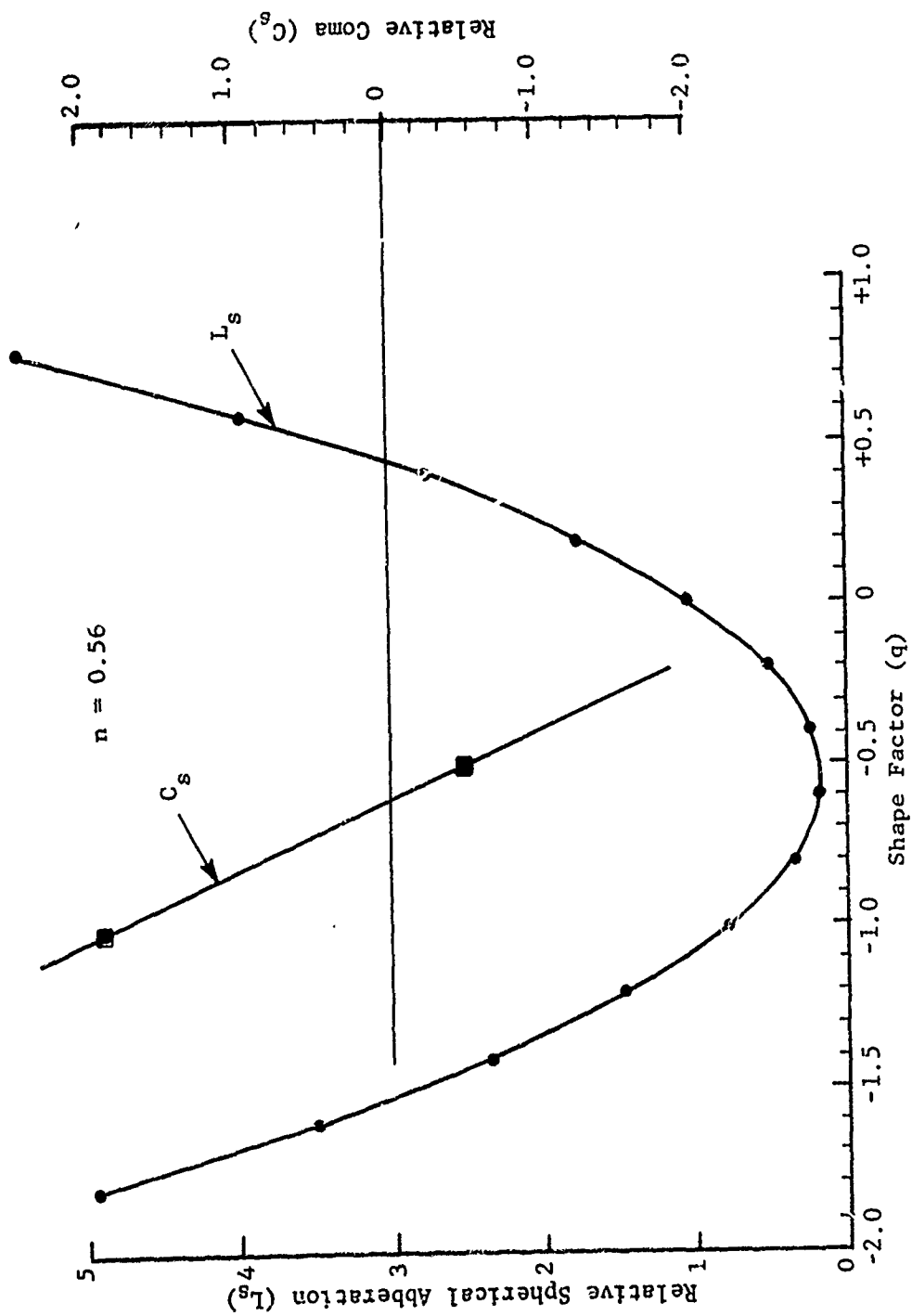


FIGURE 9. RELATIVE SPHERICAL AND COMATIC ABERRATIONS AS A FUNCTION OF SHAPE FACTOR

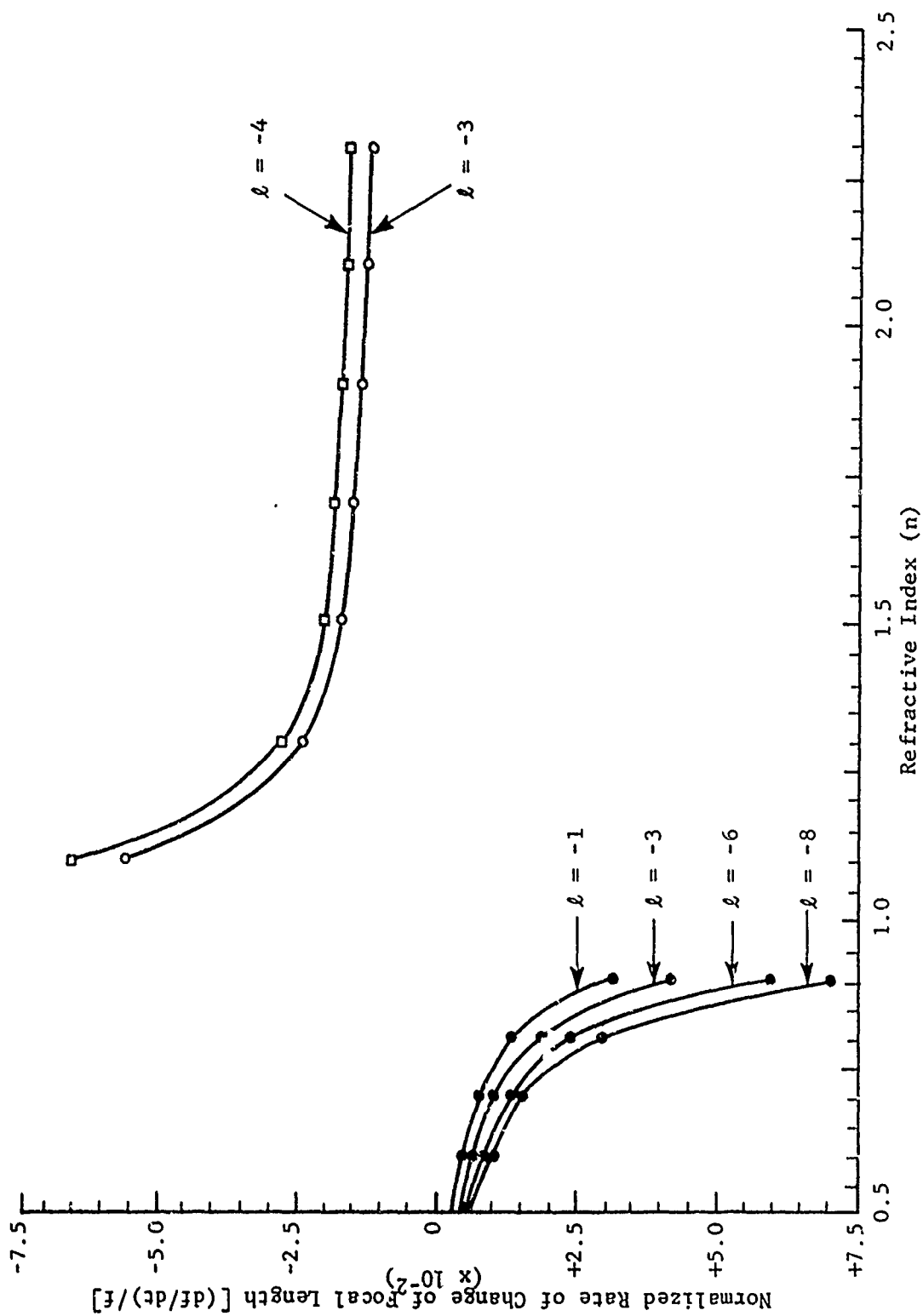


FIGURE 10. NORMALIZED RATE OF CHANGE OF FOCAL LENGTH AS A FUNCTION OF REFRACTIVE INDEX AND THERMAL COEFFICIENT OF SOUND VELOCITY

$$0.005f < df/dt < 0.05f; n' < 0,$$

$$0.05f < df/dt < 0.01f; n' > 0,$$

which is the same range as the single refracting surface liquid lens.

Using Equation (6) for ΔF and the relationship

$$\Delta T = \Delta F / (df/dt)$$

then the temperature range over which the lens will retain good focusing is given by

$$T = \pm [1.5 F_N / (D/\lambda)] \cdot [C_0(n' - 1)/n'_0(4 - \ln n'_0)] . \quad (16)$$

Off-Axis Imagery

The image quality for off-axis objects is controlled by aberrations. The off-axis aberrations contributing to degradation of the directional response are spherical aberration, coma, and astigmatism. It has been shown that spherical aberration and coma can be minimized by proper lens design; however, astigmatism cannot be controlled in the thin lens. The blur circle diameter, β (radians), contributions are given by the following relationships (Reference 8)

$$\beta_{sa} = \frac{1}{F_N^3} \left[\frac{1}{32(n'-1)^2} \right] \left[n'^2 - (2n'+1)C'' + \left(\frac{n+2}{n}\right) C''^2 \right]$$

$$\beta_{coma} = \theta / [16(n'+2)F_N^2]$$

$$\beta_{astig} = 0.5\theta^2 / F_N$$

where $C'' = (1/r_1)/(1/r_1 - 1/r_2)$ and θ is the off-axis angle in radians. The total blur circle is the sum of the three contributions. This sum is computed and plotted in Figure 11 as a function of θ , using polystyrene lens parameters from Table 1. A rule of thumb in lens design is that the lens should not be designed with an expectation of the diffraction pattern null-to-null width being less than the blur spot. However, if some degradation of the diffraction pattern in the form of increased side lobe levels is acceptable, then null-to-null widths of near one-half the blur diameter can be achieved. As an example of the use of this figure, one may conclude that well-defined diffraction patterns having a null-to-null angular width of 0.2 degrees could be expected at 10 degrees off-axis using an $f/4$ lens, and, with some degradation in response shape, a 0.1 angular degree null-to-null width could be achieved.

(Text Continued on Page 21)

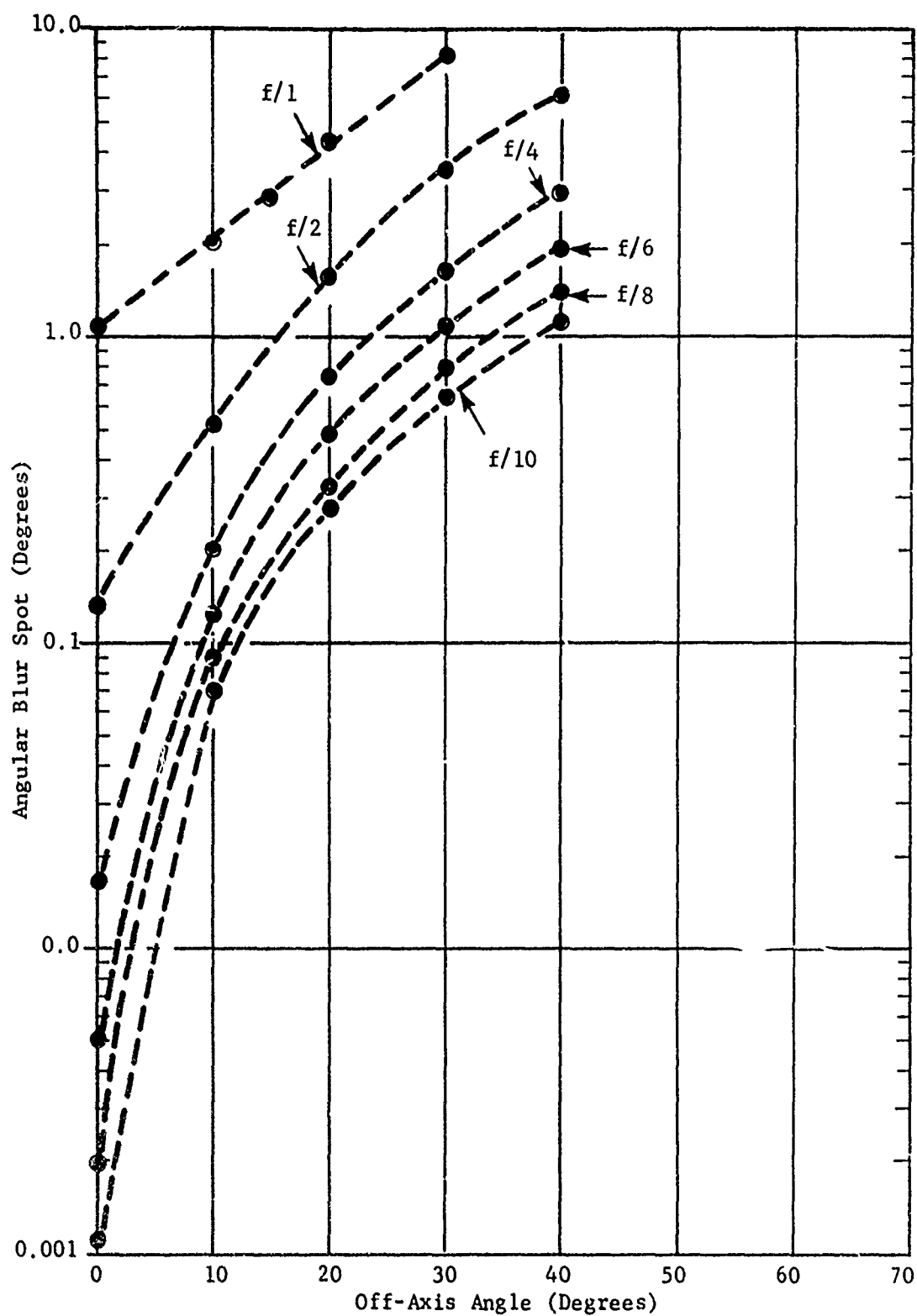


FIGURE 11. MAXIMUM BLUR SPOT DIAMETER AS A FUNCTION OF OFF-AXIS ANGLE AND f /NUMBER

TABLE 1
SOLID LENS DESIGN PARAMETERS

($C_0 = 1422$ m/sec)

Material	n'_0	n'_{15}	r_1 (meters)	r_2 (meters)	$\frac{1.5 C_0 (n'_0 - 1)}{n' (4 - 2n'_0)}$
<u>Solids</u>					
Nylon-101	0.525	0.557	-1.92	0.575	-321
Syntactic Foam	0.549	0.576	-1.75	0.557	-498
Linear Polyethylene	0.555	0.599	-1.58	0.536	-216
UHMW Polyethylene	0.600	0.648	-1.25	0.489	-180
Crystal Polystyrene	0.608	0.639	-1.31	0.498	-277
PPO	0.619	0.652	-1.23	0.485	-251
Polyethylene ($\rho=0.92$)	0.622	0.688	-1.02	0.447	-123
LEXAN	0.622	0.665	-1.15	0.472	-194
ABS	0.626	0.664	-1.15	0.473	-210
Polypropylene	0.633	0.675	-1.10	0.462	-190
PRC 1933-2 Silicone Rubber	1.498	1.625	0.656	-13.17	85
<u>Liquids</u>					
N-Methyl Glycine Sodium Salt (30% Aq)	0.744	0.782	-0.603	0.340	-144
Fluorolube Grade FS-5	1.538	1.673	0.680	-68	85
Freon-113	1.806	2.000	0.800	3.98	85
FC-75	2.154	2.408	0.886	2.390	98

Image Surface Curvature

Conrady (Reference 9) gives the curvature of field in its most general form as

$$\frac{1}{r_i} = \sum_j \frac{n_j - 1}{n_j} C_j'$$

where n_j is the index of refraction of the j^{th} lens element and C_j' is the total lens curvature ($1/r_1 - 1/r_2$) of the j^{th} lens in the lens system. For the thin lens in water, the radius of curvature of the image surface is given by $r_i = f \cdot n$ where f is the thin lens focal length and n is its index of refraction.

Typical Designs

Table 1 gives a list of lens designs for various materials assuming $f = 1$ meter and $p = -1$. The last column of this table gives a value for the second term of Equation (16). This value is a measure of the relative thermal aberration. Syntactic foam, PPO, nylon, and polystyrene will be the optimum materials in this respect and, as mentioned previously, these materials also have low attenuation values, and therefore appear to be the best choice for thin solid lenses.

Theoretical Directional Response

Figure 12 illustrates the effects of temperature variations on the directional response. In this figure, theoretical directional response is plotted at three temperatures for a nylon lens where $F_N = 2.8$ and $D/\lambda = 76$ for both the on-axis and 15 degrees off-axis conditions. Equation (16) predicts an allowable temperature variation of $\pm 10^\circ\text{C}$ range. Appendix B describes the procedure employed to compute directional responses for thin lenses.

THIN LENS IN NONAQUEOUS MEDIUM

Lens Description

When the medium in image space is not water; i.e., ($n'' \neq 1$), then the lens in Figure 13 results. With a second refractive index available as a design parameter, it is possible to design thermally corrected lenses; i.e., essentially no focal length variation with temperature.

(Text Continued on Page 23)

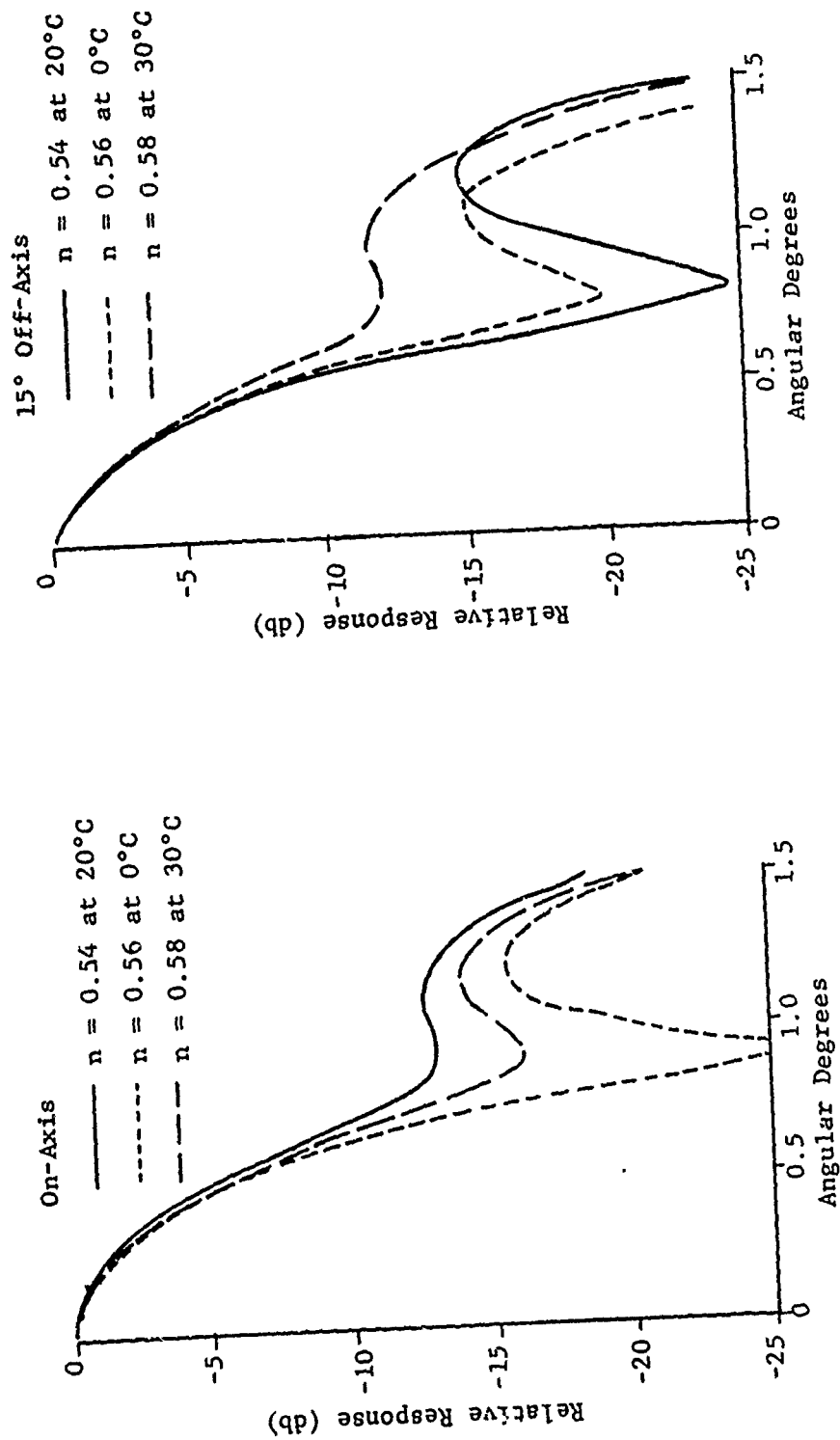


FIGURE 12. THEORETICAL DIRECTIONAL RESPONSE FOR NYLON THIN LENS
AT 0°C , 20°C , AND 30°C FOR ON-AXIS AND 15° OFF-AXIS

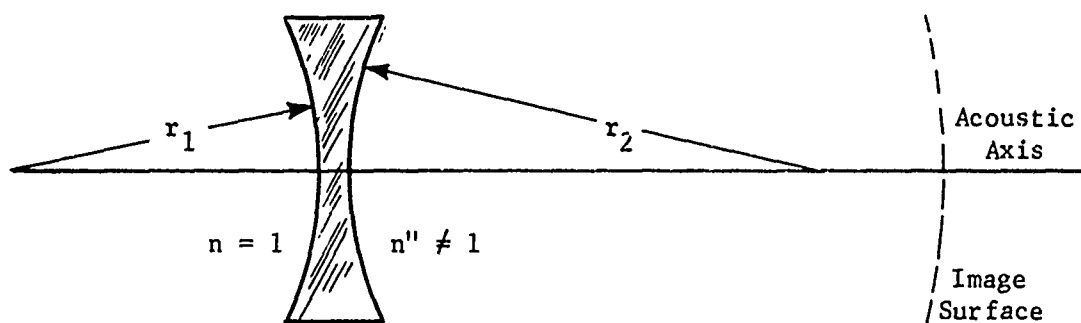


FIGURE 13. GEOMETRY OF THIN LENS IN NONAQUEOUS MEDIUM

Thermal Aberration Correction

Consider the lens equation

$$n''/f'' = (n' - n)/r_1 + (n'' - n')/r_2 \quad (17)$$

allowing $P = 1/f''$,

$$A = (n' - n)/n'',$$

and

$$B = (n'' - n')/n'',$$

then,

$$P = A/r_1 + B/r_2 .$$

Adding subscripts to A, B, and P to represent temperature in degrees Centigrade, three equations may be written as

$$P_T = A_T/r_1 + B_T/r_2 \quad T = T_1, T_2, T_3 \quad (18)$$

Temperatures of 0°, 20°, and 30°C were selected because they are representative of the temperatures encountered in the ocean.

Using the three simultaneous equations in Equation (18), it is required to solve for radii of curvature and indices which will result in $P_0 = P_{20} = P_{30}$. First, require that $P_0 = P_{30}$, then Equation (18) results in the ratio

$$r_1/r_2 = (A_0 - A_{30})/(B_{30} - B_0) .$$

Assuming P_{20} is a known requirement of the lens design then

$$P_{20} = A_{20}/r_1 + B_{20}/r_2 .$$

Combining the above two equations yields

$$r_1 = (1/P_{20}) \cdot [B_{20}(A_0 - A_{30})/(B_{30} - B_0) + A_{20}]$$

$$r_2 = r_1 \cdot (B_{30} - B_0)/(A_0 - A_{30}) .$$

For given materials it is possible to uniquely determine values of r_1 and r_2 such that $f_0 = f_{20} = f_{30}$. Experience has shown that this correction is adequate to maintain good focusing over the entire temperature range.

Additional insight may be gained into the design constraints by examination of the terms A and B. Let $b_1 = d'_n/dt$, $b_2 = dn''/dt$, and $n = 1$, then

$$B_{30} - B_0 = 30(-n_0''b_1 + n_0' b_2)/(n_0'' n_{30}'')$$

$$A_0 - A_{30} = 30(-n_0''b_1 + (n_0' - 1) b_2)/(n_0'' n_{30}'')$$

Defining quantities $a = b_1/b_2$ and $K = -n_0'' a + n_0'$ the equations for the radii of curvature may be written

$$r_1 = (1 + (a-1)/K) \cdot f_{20}$$

$$r_2 = (1 + a/(K-1)) \cdot f_{20} \quad (19)$$

also,

$$r_1/r_2 = (K-1)/K.$$

To relate these results to available materials, the general optical design rule of achieving a low total lens curvature is used. Total lens curvature is defined as $C' = 1/r_1 - 1/r_2$. Thus, using Equation (19),

$$C' = P_{20}/(K + a - 1) .$$

To achieve a low value of C' , $(K + a)$ is required to have an extreme value. This term may be written

$$K + a = n_0' + a(1 - n_0'')$$

and can be maximized by selecting materials which give large values of n_0' and a small value for n_0'' . These conditions can be satisfied, but result in a liquid as the first lens component and a solid for the second medium. This would not be good practice because coupling transducer elements to the solid would be a serious problem. For this reason, another approach to the design of this lens type must be followed because the constraint of low total curvature does not yield a useful lens design. The approach discussed in the next section does yield a thermally corrected wide-angle lens which will operate over a useful temperature range.

Typical Design

A more useful lens type results when two liquids are employed for the separate components, and the first surface is constrained to be planar; i.e., $r_1 = \infty$. This required $K = 0$, or $a = n_0'/n_0''$. Rewriting a as b_1/b_2 , then r_1 will become infinite when $\ell_1/\ell_2 = n_0''/n_0'$, and r_2 will be given by

$$r_2 = (1 - a) f_{20} . \quad (20)$$

A lens of this design is shown in Figure 14.

To achieve distortion-free images, one additional constraint should be imposed on refractive index n' . In Figure 15 observe that the relationship between angle of wavefront arrival θ and focal angle ϕ is given by Snell's law

$$\sin \phi = (\sin \theta)/n' .$$

Distortion results when $\theta \neq \phi$ or $n' \neq 1$. Therefore, to reduce image distortion, the value of n' should approximate 1 at the median operating temperature.

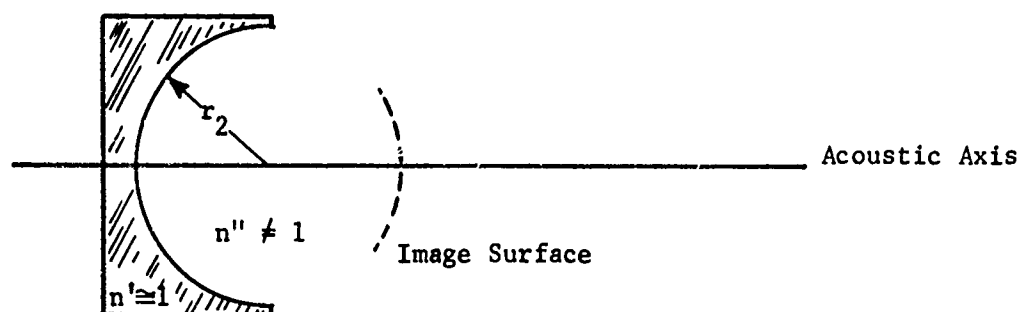


FIGURE 14. GEOMETRY OF LENS DESIGN WITH NEUTRAL ELEMENT

It is interesting to rewrite Equation (17) considering the design constraints imposed. The following relationship results:

$$f = r_2 n'' / (n'' - 1).$$

Comparing this with Equation (2) reveals that this lens is governed by the same relationships as the single refractive surface lens. The first component is a neutral element yielding thermal compensation with negligible introduction of distortion or other aberrations.

Construction Materials. There are materials which have parameters satisfying the constraints imposed above. Consider the list in Table 2.

Reference 10 lists a number of liquids which will satisfy the conditions listed in Table 2. For values of n_0'' exceeding 2, the values of k_1 exceed realizable values for liquids, therefore, solids must be considered. However, solids with extreme thermal coefficients of sound velocity values have high attenuation.

(Text Continued on Page 28)

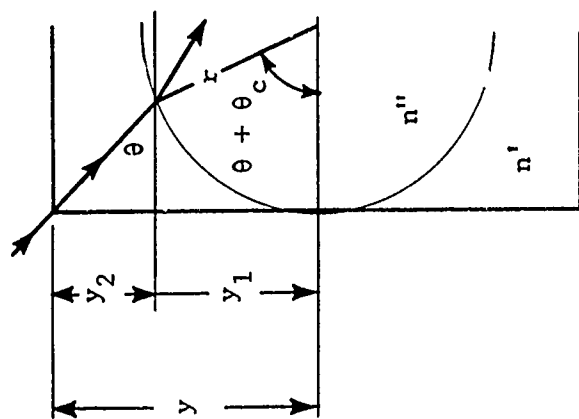
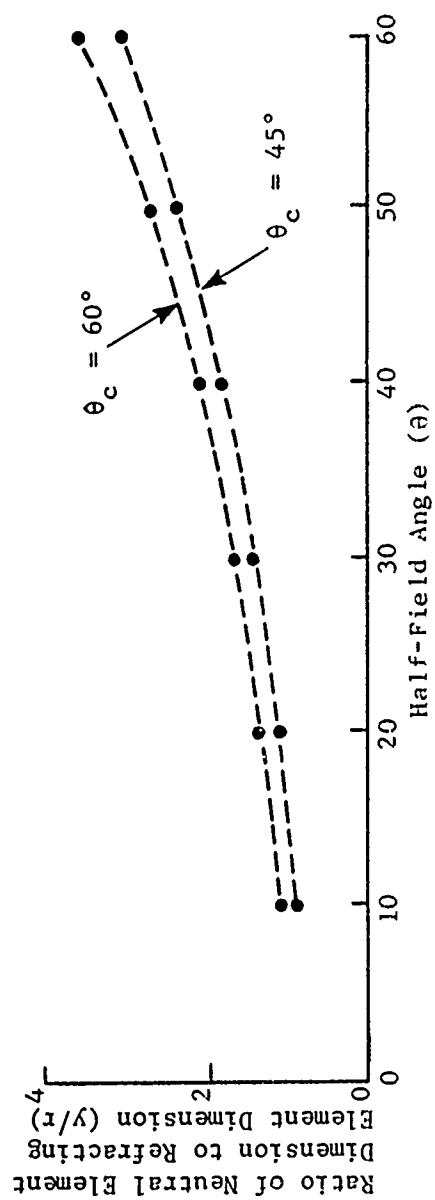


FIGURE 15. DIMENSIONS OF NEUTRAL ELEMENT TO PREVENT APERTURE BLOCKING

TABLE 2
TYPICAL LENS DESIGN PARAMETERS

n'	n''	ℓ_1	ℓ_2	a	r_2
1	1.2	-3.5	-2.9	0.833	0.166f
1	1.4	-3.5	-2.5	0.714	0.286f
1	1.6	-4.0	-2.5	0.625	0.375
1	1.8	-4.8	-2.65	0.555	0.445f
1	2.0	-5.0	-2.5	0.500	0.500f

Aperture Blocking

For wide field of view applications, the aperture dimensions of the neutral element must be large compared to the second element to eliminate aperture blocking of off-axis rays. Referring to Figure 15, it can be shown that

$$y/r = (y_1 + y_2)/r = \sin(\theta + \theta_c) + [(1 - \cos(\theta + \theta_c))] \cdot \tan \theta.$$

In this figure, θ_c is the effective lens aperture and θ is the half-field angle. There is also a plot of y/r for values of θ and θ_c in Figure 15. As an example, using $\theta_c = 45$ degrees, then for a ± 50 -degree field of view a neutral element aperture of 2.3 times the focusing aperture is required.

A lens of this type was designed for use in a high resolution imaging system.

DOUBLET THIN LENS

Description

The doublet type lens offers the designer even greater flexibility in aberration correction. Thermal aberrations as well as spherical aberration and coma may be controlled. The form of this type lens with the parameters available to the designer are shown in Figure 16. In this example $r_2 = r_3$. While this form reduces the number of degrees of

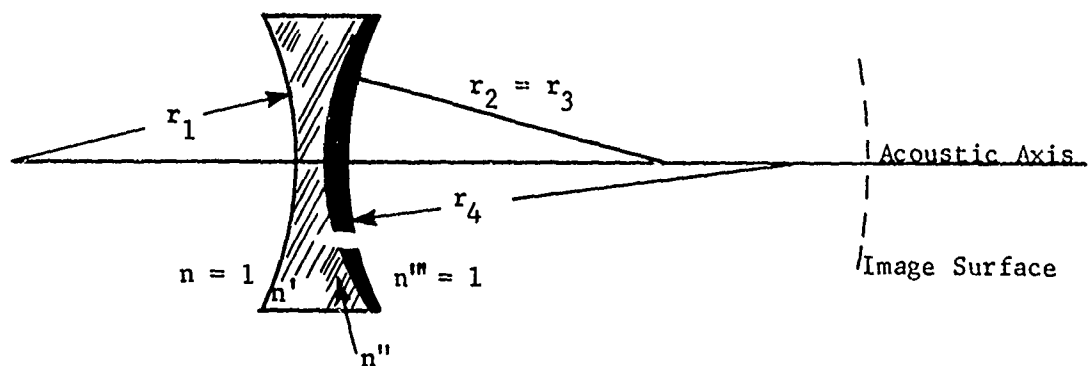


FIGURE 16. GEOMETRY OF DOUBLET THIN LENS

freedom, it also simplifies lens construction considerably as will be shown later. The second element material will generally be a low velocity soft rubber or liquid. This makes the choice of $r_2 = r_3$ even more desirable. The element thicknesses are available parameters for the optical designer, but for the acoustic lens the losses are such that a minimum thickness of the elements compatible with other parameters will generally be required.

Thermal Aberration Correction

The following analysis is based on chromatic aberration correction for optical lenses presented in Reference 7.

The lens design is begun by selecting three temperatures 0° , 15° , and 30°C at which thermal correction is required. Sometimes 20°C is substituted for 15°C because there are often data for this temperature. By requiring the focal length to be the same at all three temperatures, adequate correction is observed over the entire temperature range.

For the doublet thin lens design, it is necessary to use the relationship governing the resultant focal length of lens elements in contact:

$$\frac{1}{f} = \frac{1}{f'} + \frac{1}{f''} \quad (21)$$

where

$$\frac{1}{f'} = (n' - 1) \left[\frac{1}{r_1'} - \frac{1}{r_2'} \right]$$

and

$$\frac{1}{f''} = (n'' - 1) \left[\frac{1}{r_1''} - \frac{1}{r_2''} \right].$$

The singly primed parameters refer to the first element. The doubly primed parameters refer to the second element, and the unprimed parameters refer to the combination. Rewriting these relationships using the power relationship $P = 1/f$ and adding subscripts to designate temperature

$$P_T = (n_T' - 1) K' + (n_T'' - 1) K''; T = T_1, T_2, T_3 \quad (22)$$

where $K = (1/r_1 - 1/r_2)$ and T_1, T_2, T_3 represent three temperatures selected by the designer. For ease in presentation the temperatures 0° , 20° , and 30°C are used.

Requiring that $P_0 = P_{20} = P_{30}$, then

$$\frac{P_{20}''}{P_{20}'} = -v''/v',$$

where

$$v' = (n_{20}' - 1)/(n_{30}' - n_0'),$$

and

$$v'' = (n_{20}'' - 1)/(n_{30}'' - n_0'') \quad (23)$$

The parameters v' and v'' correspond to optical dispersion coefficients in optical lens design.

Using these relationships, the powers of the component lenses may be written as

$$\begin{aligned} P_{20}' &= P_{20} [v'/(v' - v'')] \\ P_{20}'' &= -P_{20} [v''/(v' - v'')] \end{aligned} \quad (24)$$

The parameters K' and K'' can be computed using Equation (21).

$$\begin{aligned} K' &= P_{20}'/(n_{20}' - 1) \\ K'' &= P_{20}''/(n_{20}'' - 1) \end{aligned}$$

Knowledge of K' and K'' , and the constraint $r_2' = r_1''$ results in one equation in two unknowns:

$$K' + K'' = \frac{1}{r_1'} - \frac{1}{r_2''} \quad (25)$$

This implies that many sets of parameters r_1' , ($r_2' = r_1''$), r_2'' exist for which thermal correction will occur.

One additional constraint is required to determine which set will yield optimum performance. This may be a constraint which will minimize spherical aberration, coma, or reach some compromise between them.

Coma and Spherical Aberration Correction

The technique generally employed is to compute and plot the relative amounts of spherical aberration and coma for various sets of curvature parameters, and then selecting the set which gives the best compromise. It is important to realize, however, that these computations are based on a paraxial analysis which is only an approximation. (Further analysis is generally required to optimize the lens design. This analysis is based on evaluation of the lens directional response discussed in Appendix B.)

A method commonly used in optics is the "G-Sum" method given by Conrady on page 231 of Reference 9. A second method that is easier to compute than the "G-Sum" technique is to consider the doublet as a singlet with an effective index of refraction which will provide the focal length required; i.e.,

$$\frac{1}{f} = (N_{eff} - 1) \cdot (1/r_1' - 1/r_2'')$$

or

$$N_{eff} = 1 + P_{20}/(K' + K'')$$

also an effective shape factor

$$Q_{eff} = (r_2'' + r_1')/(r_2'' - r_1') \quad (26)$$

may be defined.

It is then possible to numerically evaluate Equations (9) and (10) for relative amounts of spherical aberrations and coma for a range of Q_{eff} values to determine the value of Q_{eff} which yields the best aberration compromise.

Employing Equations (25) and (26), it is possible to write for the lens radii of curvature,

$$\begin{aligned} r_1' &= 2/[(q + 1) \cdot (K' + K'')] , \\ r_2' &= r_1'' = r_1'/(1 - r_1' K') , \\ r_2'' &= r_1'/[1 - r_1' \cdot (K' + K'')] . \end{aligned} \quad (27)$$

where q is determined from an evaluation of Equations (9) and (10).

The shape factor technique described above does not give results identical with the "G-Sum" technique but since both methods are only approximate, either is useful for preliminary analysis. Final design should be accomplished by means of a computer using automatic lens design techniques.

Construction Materials

From Table A1 of Appendix A, it can be seen that the acoustic dispersion indices for listed solids are in the range -7 to +2.7. It has been shown in optics that better lens performance can be achieved if the curvature values of individual components can be made low; i.e., K' and K'' small. If the relationships in Equations (21) and (23) are used, the following relationships result:

$$\begin{aligned} K' &= \frac{1}{f} \cdot \left[\frac{1}{(v' - v'')(n_{30}' - n_0')} \right] \\ K'' &= \frac{1}{f} \cdot \left[\frac{1}{(v'' - v')(n_{30}'' - n_{30}') } \right] . \end{aligned}$$

These imply that for small K values, materials having extreme opposite values of dispersion index should be employed.

Again referring to Table A1, it will be found that the material PRC-1933 ($v = +2.5$) combined with Nylon ($v = -7$), Syntactic Foam ($v = -7.8$), Polystyrene ($v = -5.9$), or PPO ($v = -5.2$) are candidate materials. Acrylic is not considered due to a drastically nonlinear temperature-sound velocity relationship. Fortunately these materials are also characterized by low attenuation values. Until further materials measurements are made these appear to be the most suitable solid lens construction materials. A low sound velocity liquid such as FC-75 or Fluorolube would be a suitable replacement for PRC-1933 rubber for a solid/liquid lens combination. The advantage in using a liquid is the lower attenuation losses incurred.

Typical Designs

Using the preceding analysis, lens designs were computed using both solid/solid and solid/liquid components. The lens parameters are listed in Table 3.

TABLE 3
LENS PARAMETERS FOR ALL SOLID OR SOLID-LIQUID
LENS COMPONENTS

<u>Material</u>	<u>Material</u>	<u>r_1'</u> <u>(cm)</u>	<u>r_1''</u> <u>(cm)</u>	<u>r_2''</u> <u>(cm)</u>	<u>r_i</u> <u>(cm)</u>
Polystyrene	PRC-1933-2	-640.6	54.1	71.1	79.3
Polystyrene	FC-75	-378.0	58.6	66.7	84.0
Syntactic Foam	PRC-1933-2	-680.5	59.4	75.6	69.3
Syntactic Foam	FC-75	-488.9	62.5	69.8	72.4
Nylon 101	PRC-1933-2	-1557	61.7	81.9	78.8
Nylon 101	FC-75	-679	66.1	75.4	72.2

The material properties listed in Table A1 were employed in these calculations which yield temperature compensated lenses designed under the constraint $f_0 = f_{20} = f_{30} = 100$ cm.

TEST RESULTS

TEST FACILITY AND PROCEDURE

No experimental results are presented for the liquid-filled single refracting surface lens or for the thin lens in a nonaqueous medium. Experimental data are available in Reference 3.

Experimental data for the other lens types were obtained using a high frequency tank having dimensions of 2 meters long, 76 cm wide, and 1 meter deep.

Measurements were performed by placing the lens close to a line-array projector. Wavefronts are planar at a small distance (a few centimeters) from the projector and may be represented as plane waves from a point source in the lens far-field. Figure 17 illustrates the experimental arrangement for both the on-axis and off-axis directional response measurements. In the figure, the lens and projector are mechanically attached and the unit is free to rotate about an axis of rotation perpendicular to the page. The hydrophone mounted on an optical bench is free to move along the acoustic axis. The distance along the acoustic axis marked f in the figure is referred to in subsequent discussions. When the hydrophone is positioned at the focal point of the lens, then $f = f$.

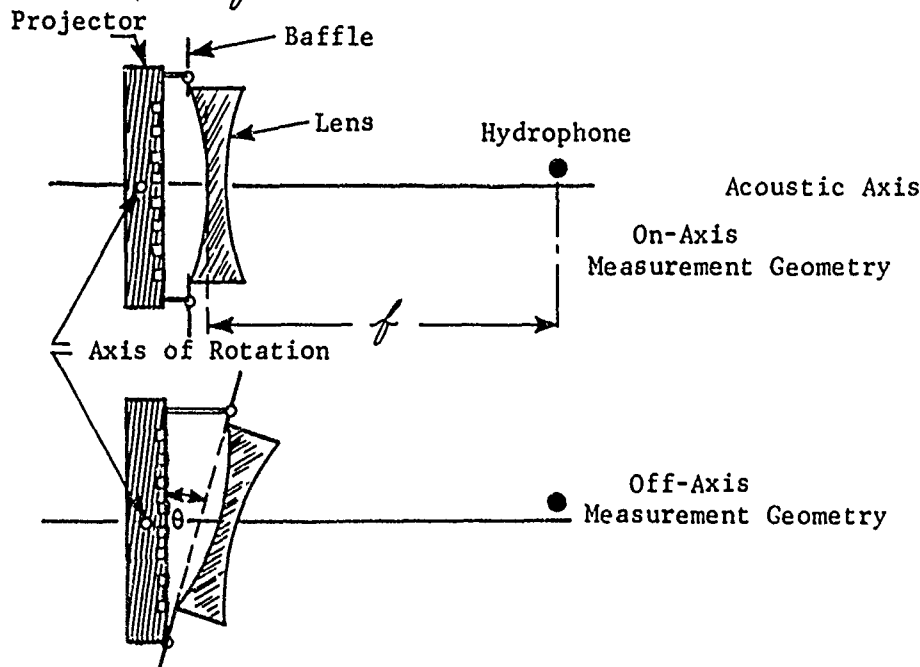


FIGURE 17. EXPERIMENTAL MEASUREMENT GEOMETRY

TEST OBJECTIVES

Several single element thin lenses have been constructed and tested. Experimental results for some of these lenses are reported here. The materials used were nylon, polyethylene (two lenses), and polystyrene. Doublet thin lenses were also constructed and tested. The doublets were fabricated using polyphenylene oxide and silicone rubber (PRC-1933-2); nylon and silicone rubber; and polyethylene and silicone rubber. The primary objectives of the experimental work were:

1. Determine the focusing properties of thin solid lenses in the frequency range 600 kHz to 1200 kHz with angular resolutions in the order of 0.5 degrees.
2. Determine if simple lenses could be designed using paraxial ray theory developed for optical lens design.
3. Determine if multi-element solid lenses would perform according to theoretical expectations if it is assumed that only refraction according to Snell's law occurs at the interfaces.

TEST RESULTS FOR SINGLET LENSES

Nylon Lens

Nylon has an index of refraction of approximately 0.56 (Table A1). The spherical aberration and coma analysis presented in Figure 9 resulted in a choice for the shape factor, $q = -0.6$. Using Equation (15), we find

$$r_1 = -2.2f, \quad r_2 = 0.55f.$$

For this lens design, a focal length (f) of 50 cm was selected, hence the resultant lens parameters are shown in Figure 18.

A clear aperture of 18 cm was chosen in order to achieve high angular resolution in the frequency range of 600 to 1200 kHz.

Employing the test geometry shown in Figure 17 and using an LC-5 hydrophone (Atlantic Research) as a test probe, the directional response was measured.

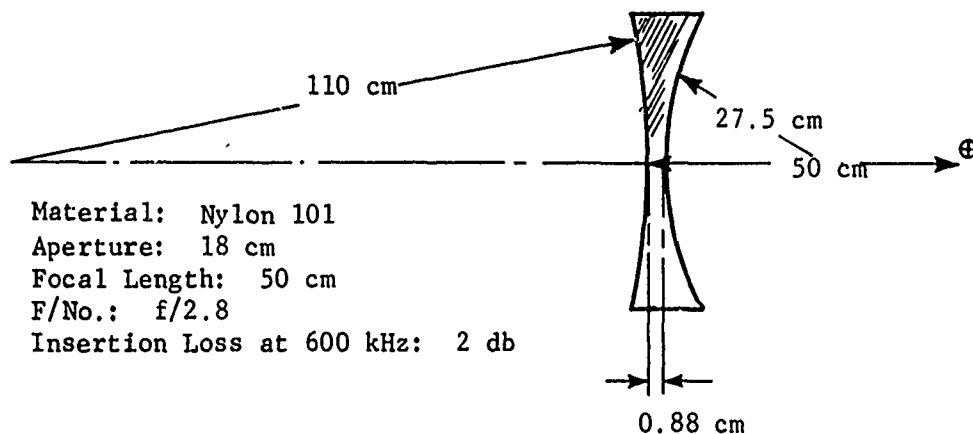


FIGURE 18. NYLON LENS PARAMETERS

Figure 19 is the theoretical on-axis amplitude plotted as a function of focal distance f . The theoretical values may be obtained from Equation (5.1) or the lens mathematical model described in Appendix B. Note that the depth of focus (defined by the -0.5 db points) is approximately 6 cm as predicted by Equation (6). That the maximum on-axis amplitude occurs at 51.5 cm rather than at the gaussian focal position of 50 cm results from the finite lens thickness not accounted for in the gaussian lens formula.

Measured on-axis directional response patterns for f values of 48.3 cm, 49.3 cm, 51.3 cm, and 54.3 cm are shown in Figure 20. These patterns indicate a depth of focus of nearly 6 cm does exist.

An expanded ($0.1^\circ/\text{division}$) directional response for $f = 50.8$ cm is shown in Figure 21. A theoretical pattern obtained by the computer program described in Appendix B is also shown for comparison. The -3 db beamwidth is approximately 0.6 degrees.

Figure 22 shows the theoretical and measured directional response for a wavefront arriving at 15 degrees off-axis to the lens. This is

(Text Continued on Page 41)

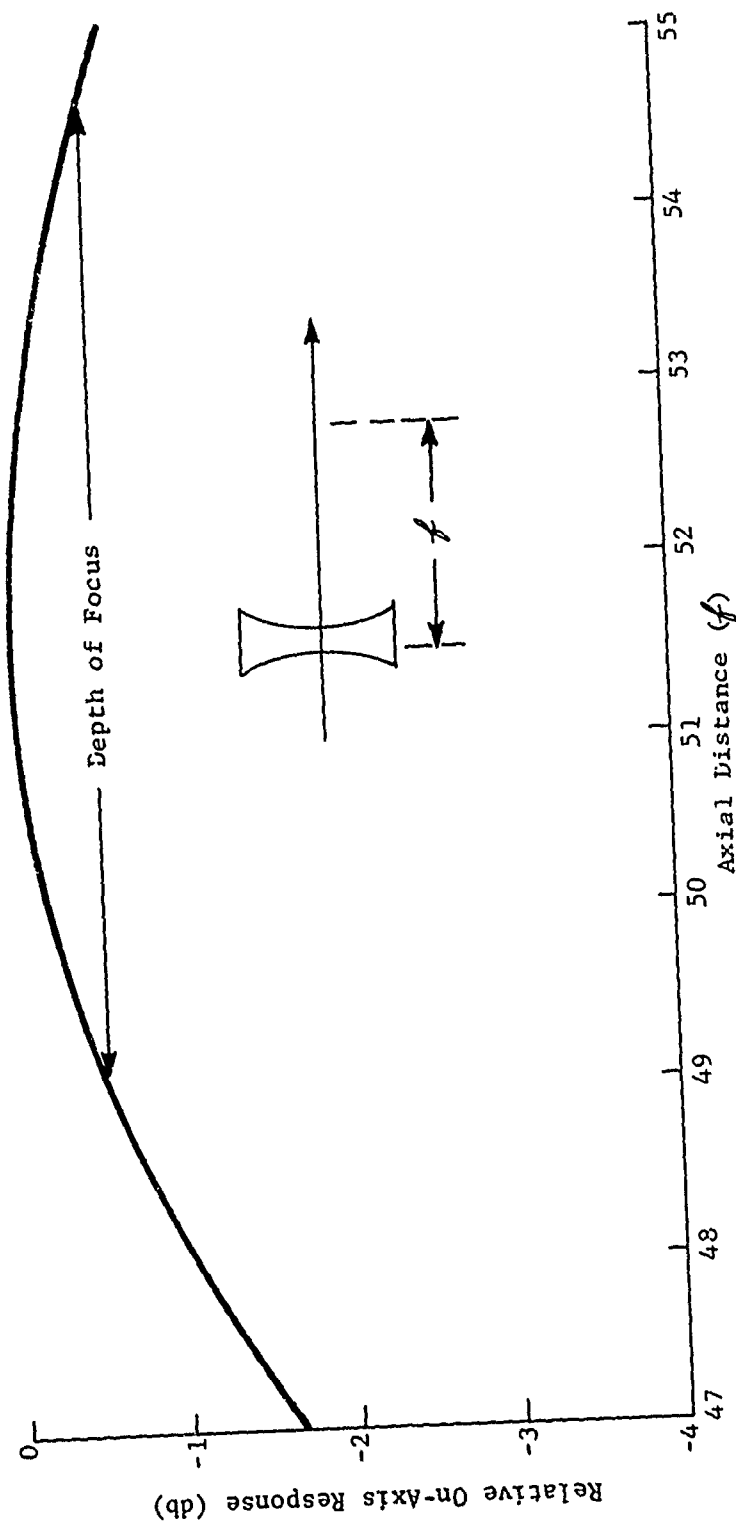


FIGURE 19. THEORETICAL AXIAL AMPLITUDE RESPONSE

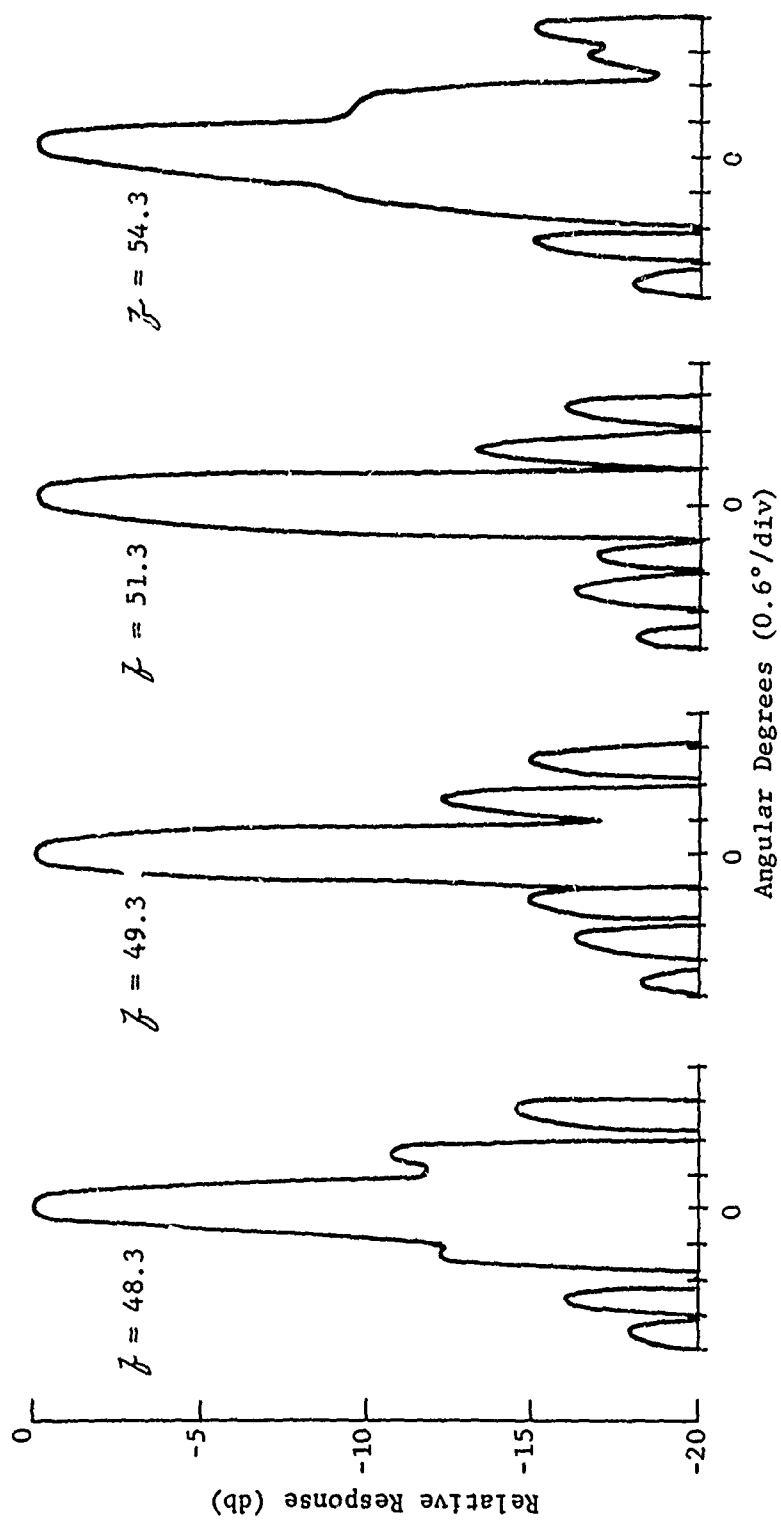


FIGURE 20. MEASURED ON-AXIS DIRECTIONAL RESPONSE AS A FUNCTION OF AXIAL POSITION (NYLON LENS)

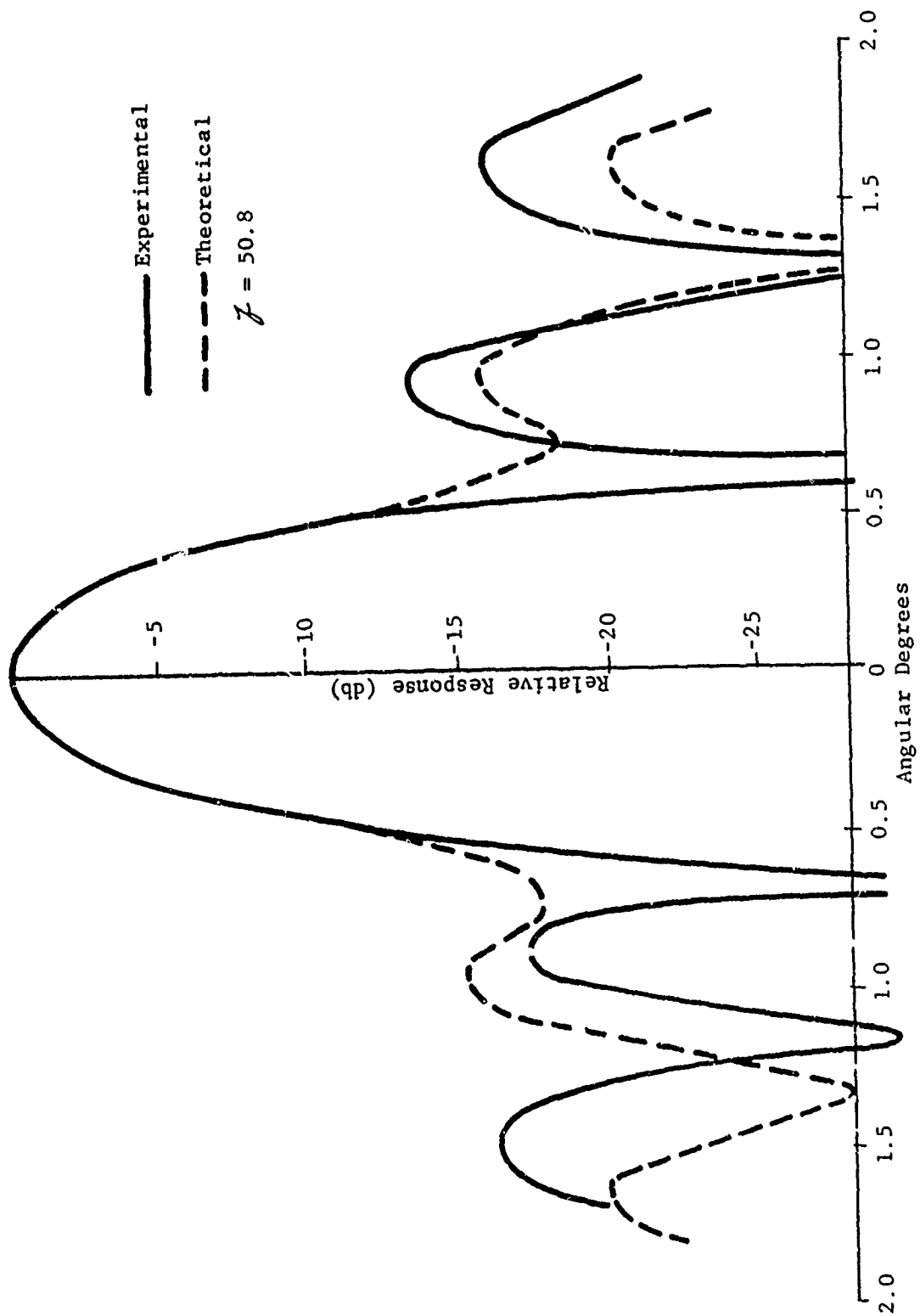


FIGURE 21. THEORETICAL AND MEASURED ON-AXIS DIRECTIONAL RESPONSE AT 600 kHz (NYLON LENS)

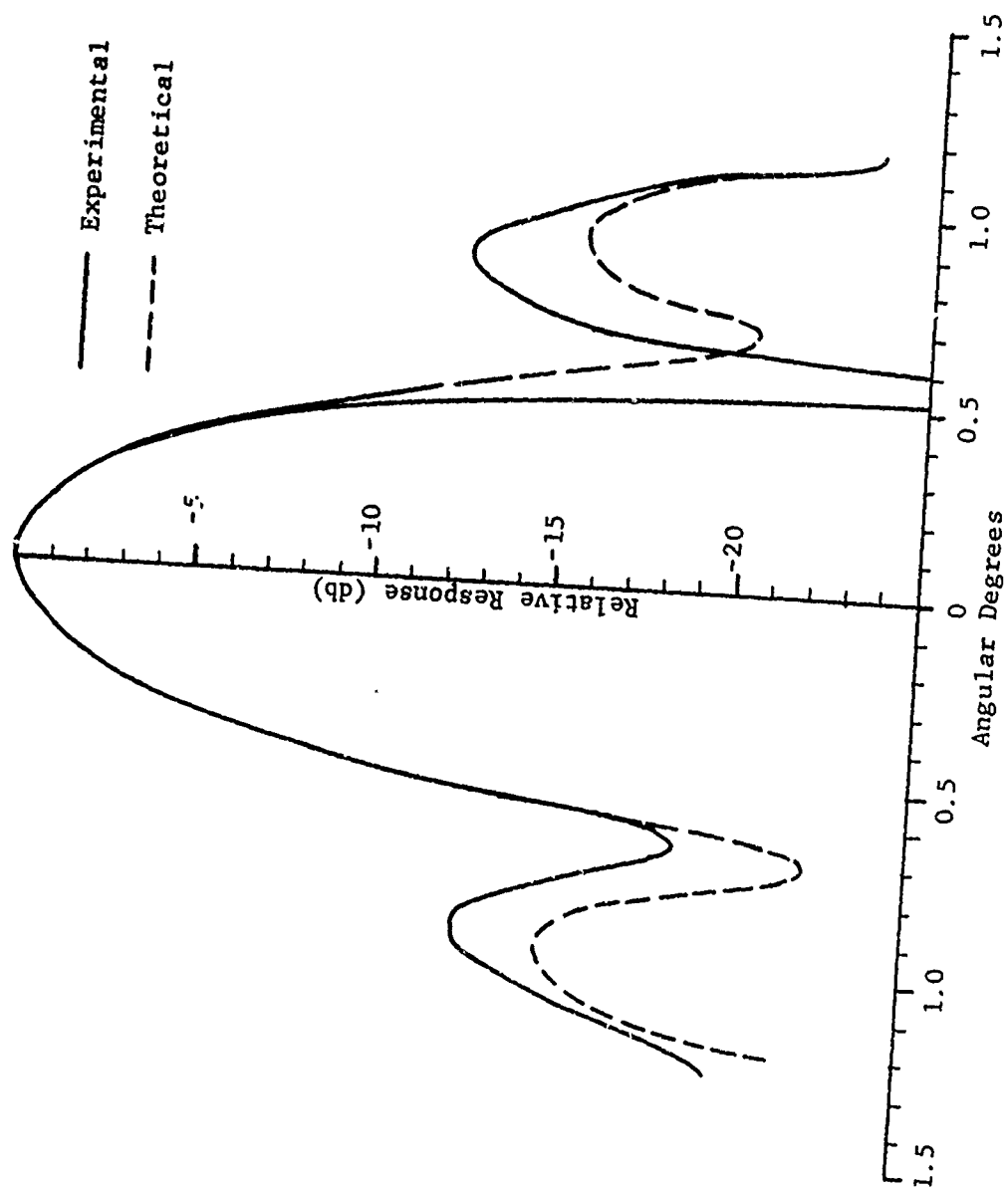


FIGURE 22. THEORETICAL AND MEASURED DIRECTIONAL RESPONSE
AT 600 kHz (NYLON LENS, 15° OFF-AXIS)

an excellent response pattern and indicates that the lens is capable of good beamforming over a total field of view of 30 degrees.

Directional responses were measured at 1052 kHz for both the on-axis and 15-degree off-axis cases to investigate the focusing properties of the lens at higher frequencies. These responses are shown in Figure 23a and 23b. At this frequency a square hydrophone element of 0.25 cm on a side was used as a receiving element. The -3 db beamwidth at this frequency is near 0.35 degrees for both cases.

Equation (8) yields a temperature range of ± 12.5 degrees over which good focusing should be maintained at a fixed value of f . No experimental validation of this characteristic was attempted but directional responses were computed to demonstrate the lens performance at temperatures of 10°C ($n = 0.54$), 20°C ($n = 0.56$), and 30°C ($n = 0.58$). These computed responses are shown in Figure 12 for both the on-axis and 15 degrees off-axis cases.

Bi-Concave Polyethylene Lenses

Two polyethylene lenses were constructed and tested. The first lens was designed for minimum coma, which, for an index of refraction of 0.7, requires a shape factor of $q = 0.4$. Equation (15) then requires that $r_1 = -1.0 f$, and $r_2 = 0.428 f$. A focal length of 50 cm was desired, therefore, $r_1 = -50$ cm and $r_2 = 21.4$ cm. Figure 24 is a cross section of the lens. As in the case of the nylon lens, a clear aperture of 18 cm was chosen. As in the case of the nylon lens, Equation (6) will yield a focal range of ± 3 cm.

Figure 25 shows measured on-axis direction response patterns for f values of 54.8 cm, 57.6 cm, and 59.8 cm at 600 kHz. These patterns confirm that the focal range is approximately ± 3 cm. The -3 db beamwidth is 0.6 degrees.

Figure 26 shows a measured directional response at 1.2 MHz. The -3 db beamwidth is approximately 0.4 degrees.

The LC-5 hydrophone was employed as the acoustic sensor at both frequencies.

The f values are larger than 50 cm which was computed from the f gaussian lens equation for two reasons: first, the lens thickness, and second, the temperature was 23°C for the measured responses. The focal length shift is approximately 0.8 cm/°C for a polyethylene lens of this type.

(Text Continued on Page 46)

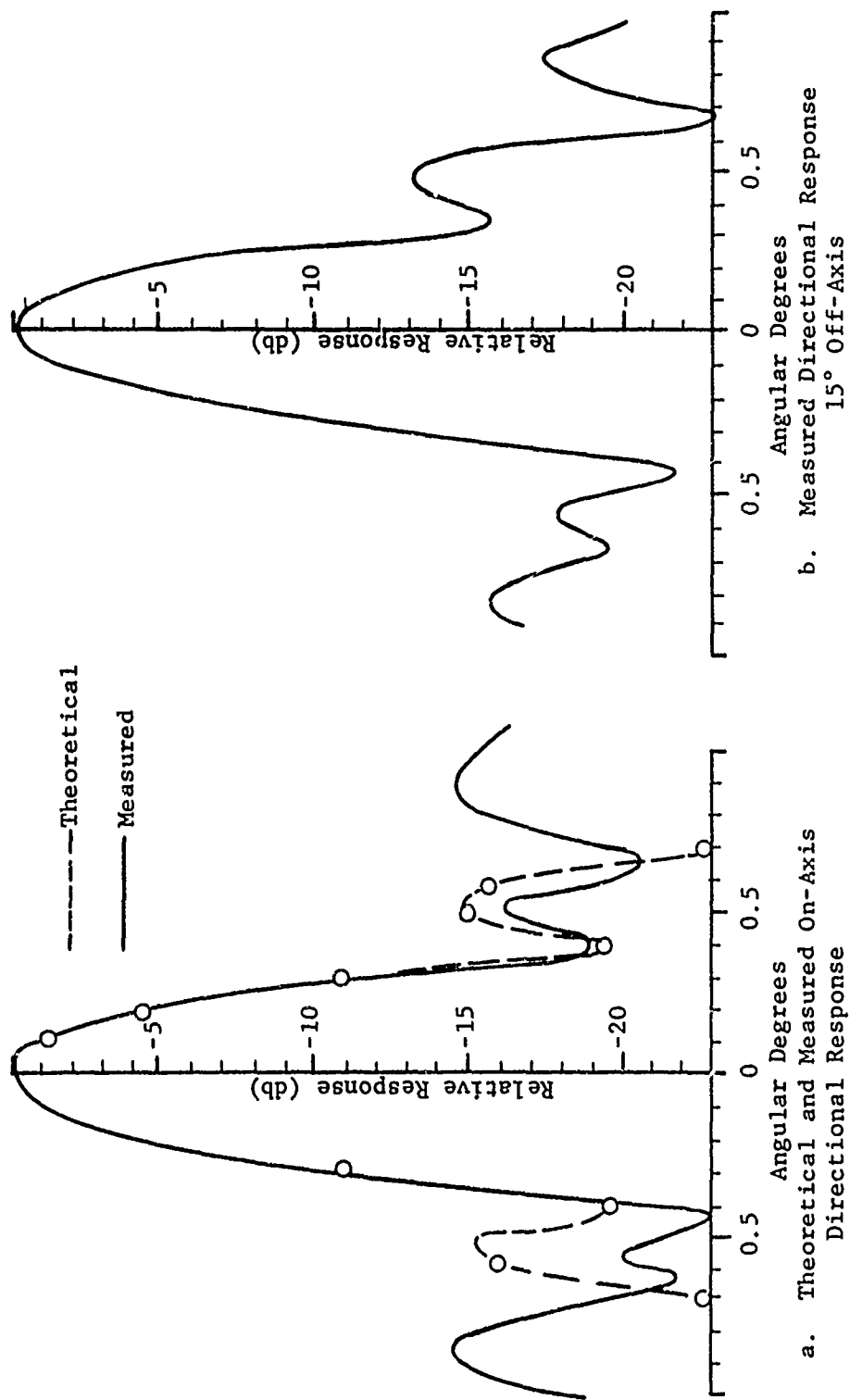


FIGURE 23. THEORETICAL AND MEASURED DIRECTIONAL RESPONSE
AT 1052 kHz (NYLON LENS)

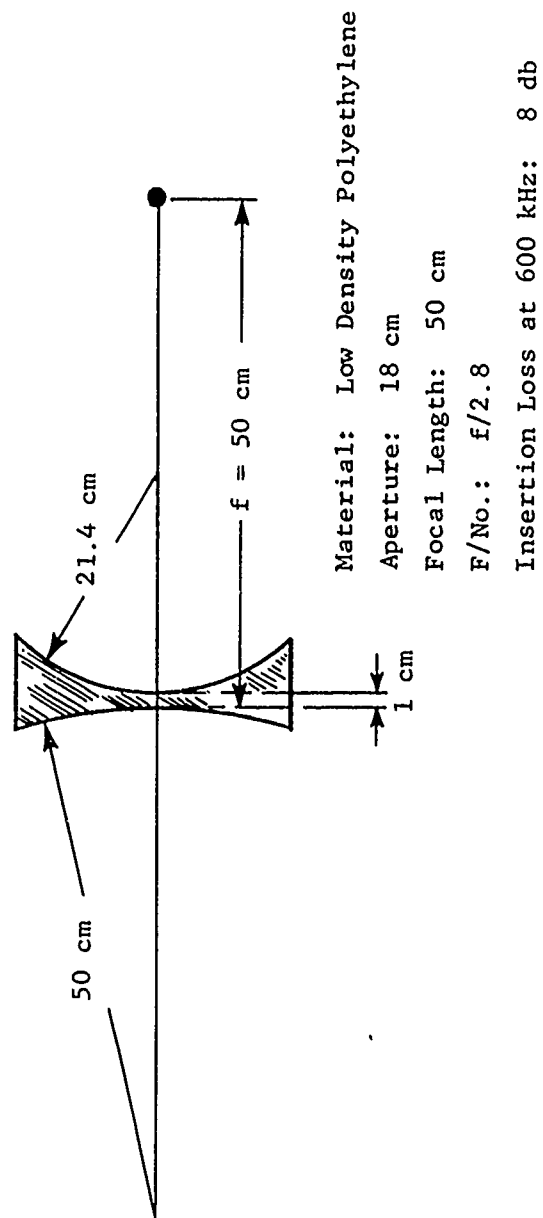


FIGURE 24. POLYETHYLENE BI-CONCAVE LENS PARAMETERS

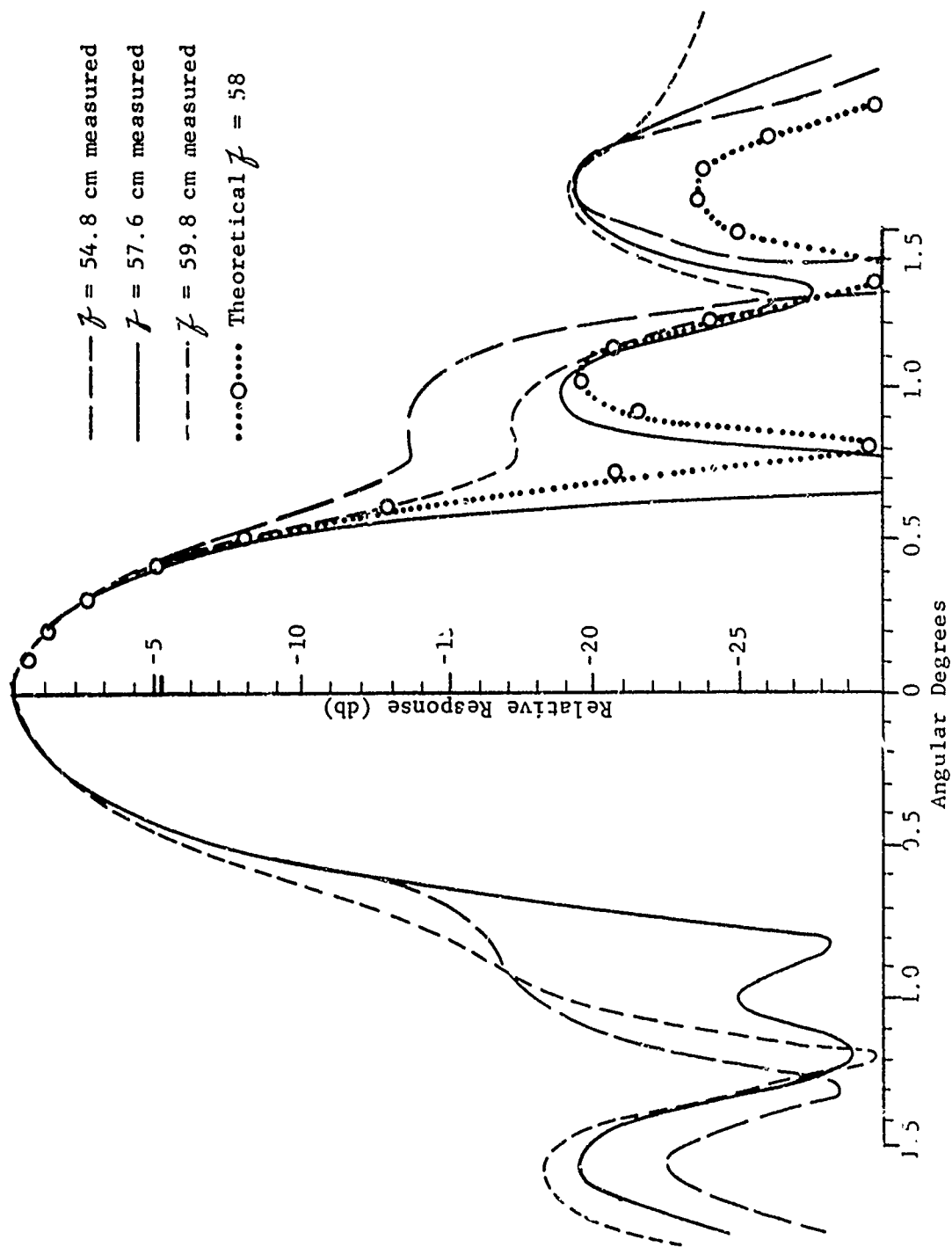


FIGURE 25. THEORETICAL AND MEASURED ON-AXIS DIRECTIONAL RESPONSE AT 600 kHz FOR THREE AXIAL POSITIONS (POLYETHYLENE LENS)

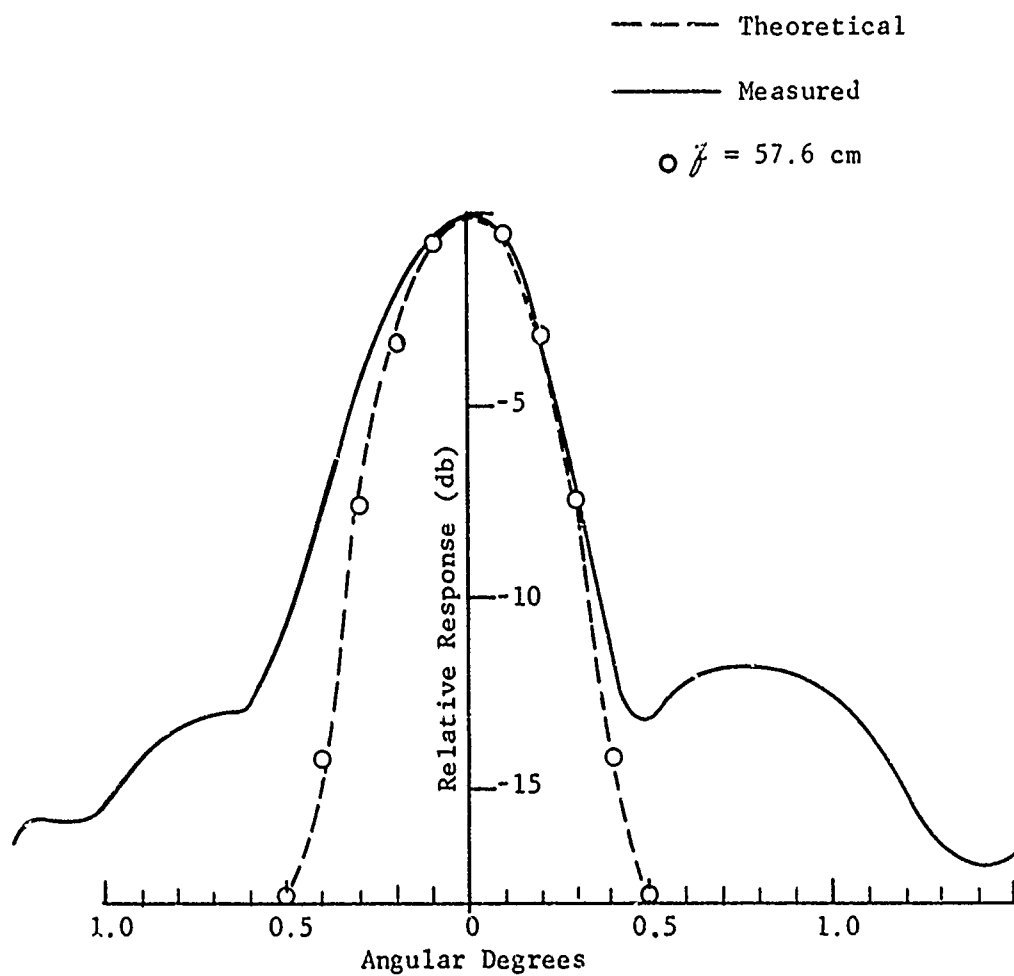


FIGURE 26. THEORETICAL AND MEASURED ON-AXIS DIRECTIONAL RESPONSE AT 1.2 MHz (BI-CONCAVE POLYETHYLENE LENS)

Plano-Concave Polyethylene Lens

A second polyethylene lens was designed with no aberration correction constraints. For this lens, one surface was chosen to be flat (plano) and the other surface selected to yield a focal length of 45 centimeters. Using the gaussian lens equation the second surface must have a radius of curvature of 13.65 cm. A drawing of this lens is shown in Figure 27.

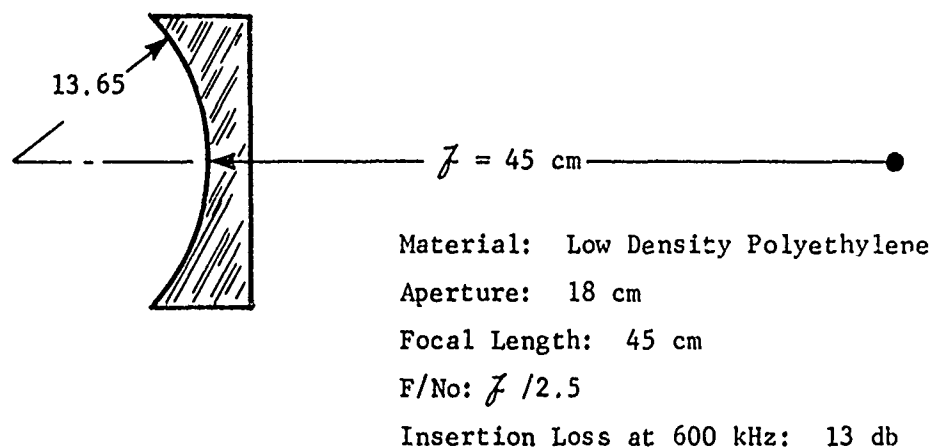


FIGURE 27. POLYETHYLENE PLANO-CONCAVE LENS PARAMETERS

Theoretical and experimental on-axis directional responses for f values of 41.5 cm, 45.5 cm, 51.5 cm, and 53.5 cm are shown in Figure 28. The -3 db beamwidth is approximately 0.6 angular degree.

Figure 29 is a 15 degree off-axis directional response measured at 600 kHz. This response implies that a total field of view of 30 degrees is practical with this lens type. The -3 db beamwidth is approximately 0.8 degree.

Polystyrene Lens

As a part of a multi-element lens system, a polystyrene lens was constructed. Since this element was not originally intended to operate

(Text Continued on Page 48)

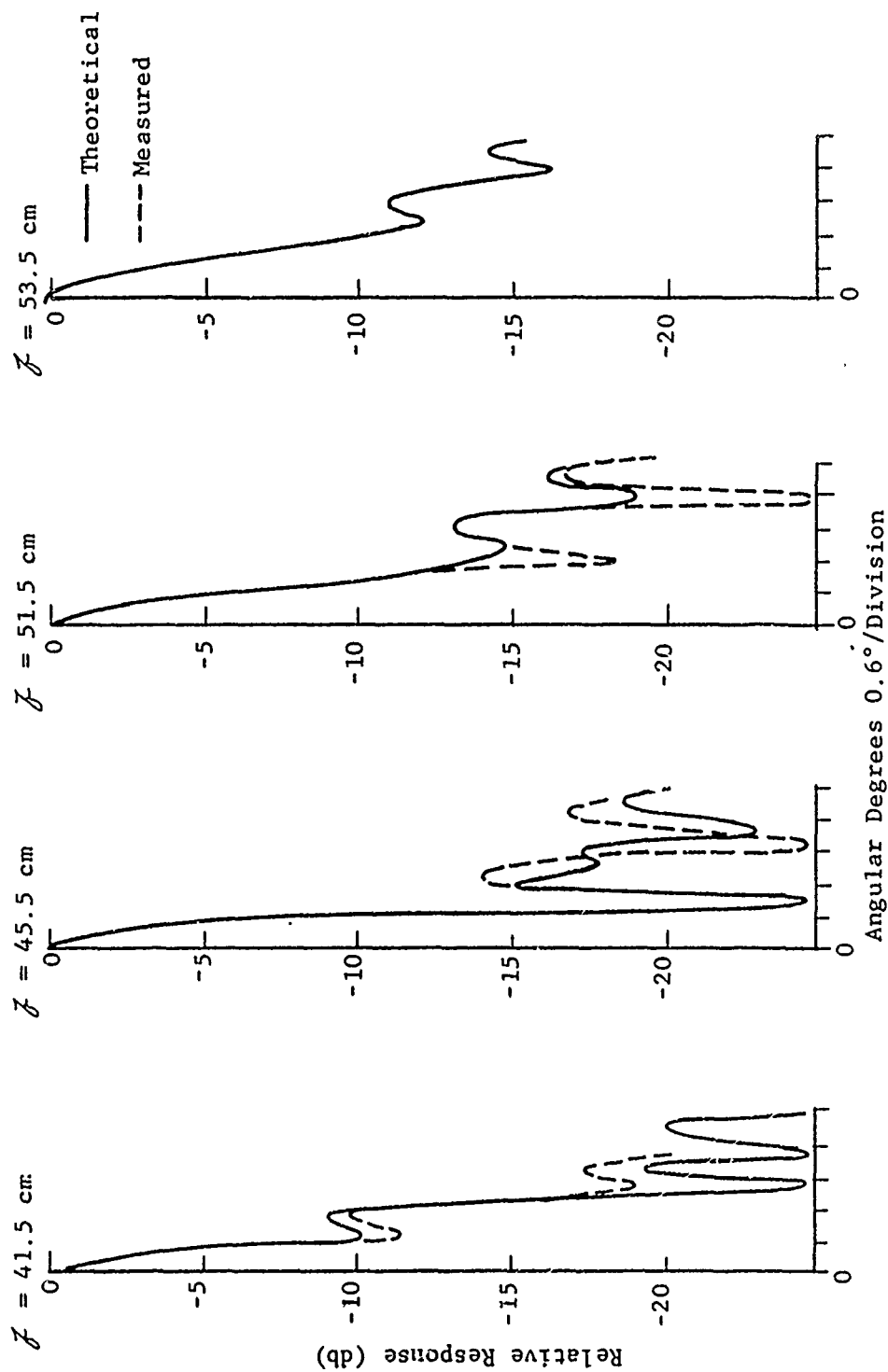


FIGURE 28. THEORETICAL AND MEASURED ON-AXIS DIRECTIONAL RESPONSE AT 600 kHz (PLANO CONCAVE POLYETHYLENE LENS)

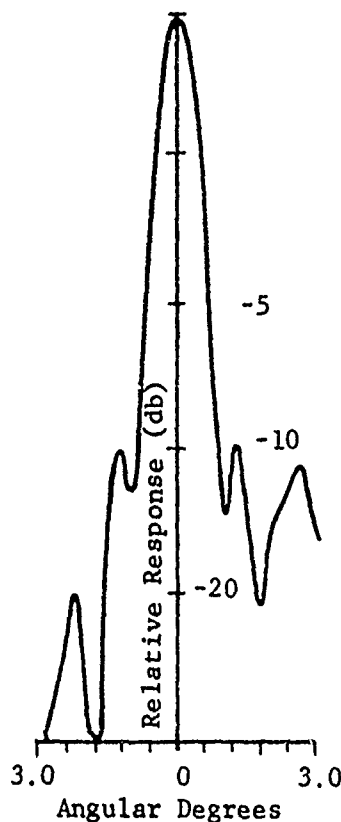


FIGURE 29. MEASURED DIRECTIONAL RESPONSE AT 600 kHz
(PLANO-CONCAVE POLYETHYLENE LENS, 15° OFF-AXIS)

as a singlet, it was not designed to minimize coma or spherical aberrations. However, to determine the characteristics of lenses constructed of polystyrene (a low absorption loss material), tests were made. The lens dimensions are shown in the cross-sectional drawing of Figure 30.

The radii of curvature of the lens are $r_1 = -64.97$ cm and $r_2 = 16.92$ cm, and the index of refraction at 20°C is 0.64. The gaussian focal length is 37.5 cm. The clear aperture is 20 cm.

According to Equation (6) the expected focal range is ± 1.5 cm and Equation (17) yields an expected temperature range of $\pm 10^\circ\text{C}$.

Figure 31 shows measured directional responses for f values of 37.5 cm, 40.5 cm, and 41.5 cm. These patterns tend to confirm that the focal range is rather narrow due to its large aperture of $f/1.8$.

Figure 32 shows an expanded directional response measured at $f = 39.5$ cm and 600 kHz for the on-axis conditions. A -3 db beamwidth of 0.55 angular degrees is indicated in this figure.

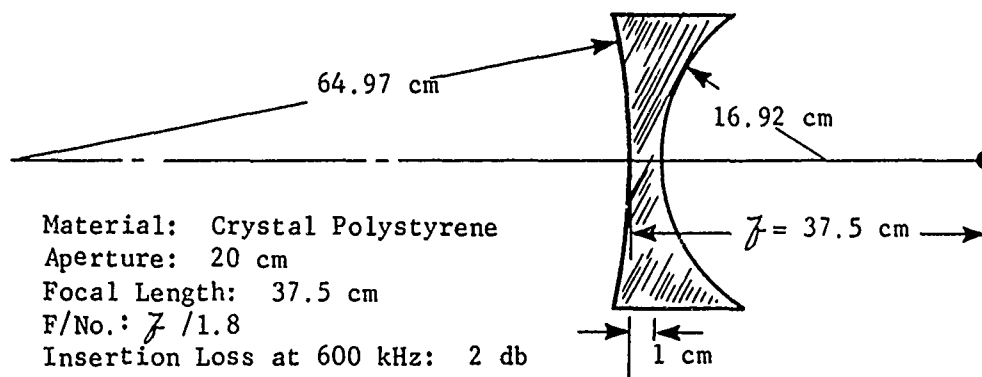


FIGURE 30. POLYSTYRENE LENS PARAMETERS

Figure 33 shows a directional response measured for wavefronts arriving at 20 degrees off-axis at 600 kHz. This implies a capability of good performance over a total field of 40 angular degrees, with a 0.6 degree beamwidth at -3 db.

Figure 34 shows a directional response measured at a 1 MHz frequency. The -3 db beamwidth at this frequency is approximately 0.35 degrees.

Off-axis patterns at 1 MHz were very poor for angles of greater than 5 degrees indicating a large amount of coma.

TEST RESULTS FOR DOUBLETS

Three doublet lenses were constructed and tested. These were constructed of polyethylene and silicone rubber, nylon and silicone rubber, and polyphenylene oxide and silicone rubber. Only the polyphenylene oxide and silicone rubber lens was designed as an athermal lens using Equations (21) through (26). The other lenses used the nylon and polyethylene singlets with one side filled with silicone rubber.

(Text Continued on Page 53)

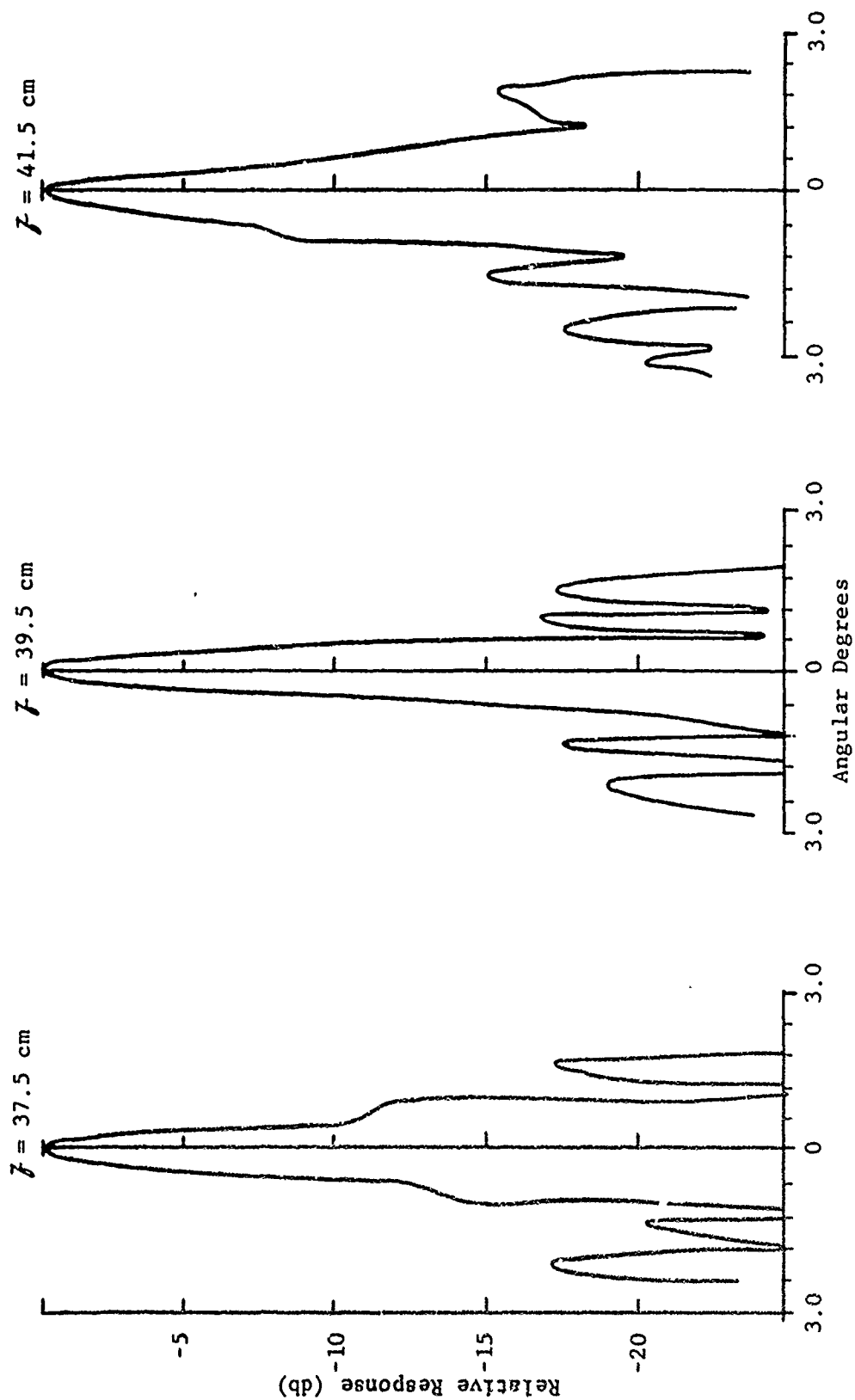


FIGURE 31. MEASURED ON-AXIS DIRECTIONAL RESPONSE AT 600 kHz AS
A FUNCTION OF AXIAL POSITION (POLYSTYRENE LENS)

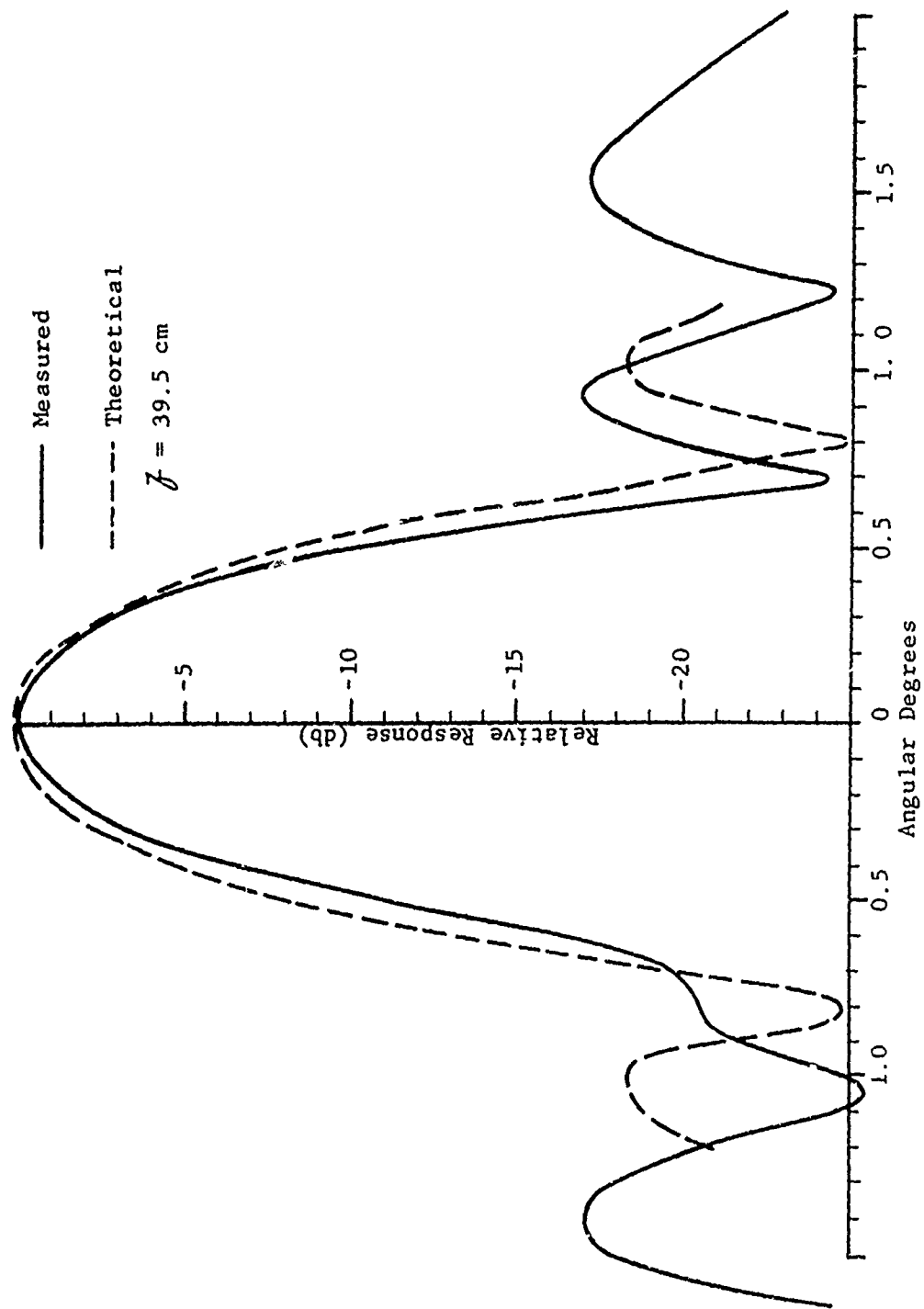


FIGURE 32. THEORETICAL AND MEASURED ON-AXIS DIRECTIONAL RESPONSE
 AT 600 kHz (POLYSTYRENE LENS)

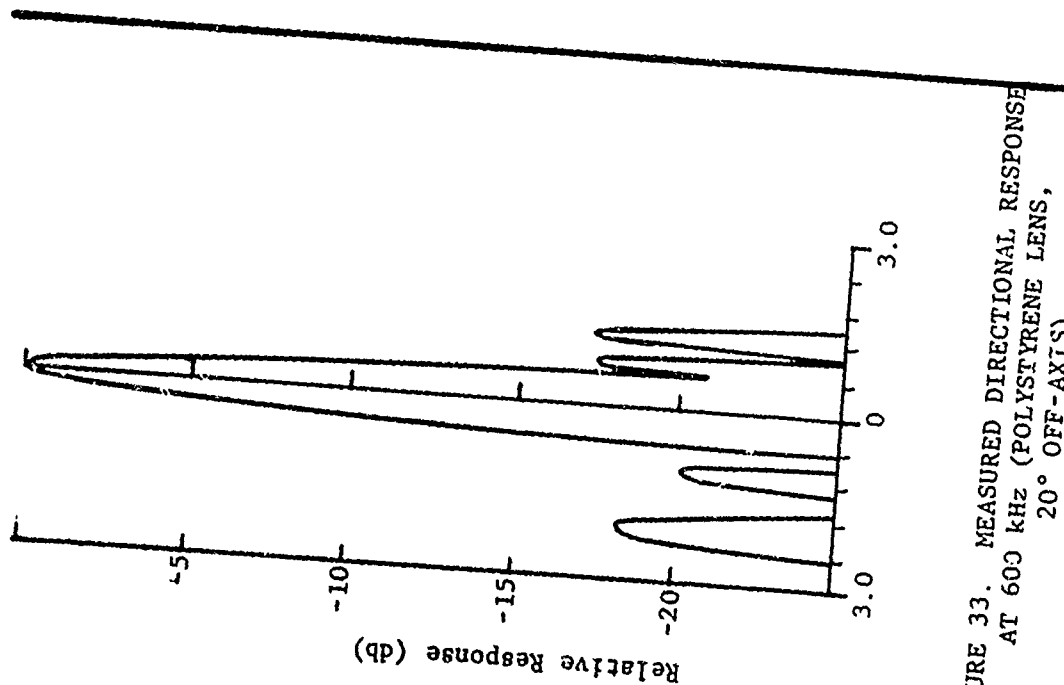


FIGURE 33. MEASURED DIRECTIONAL RESPONSE
AT 600 kHz (POLYSTYRENE LENS,
20° OFF-AXIS)

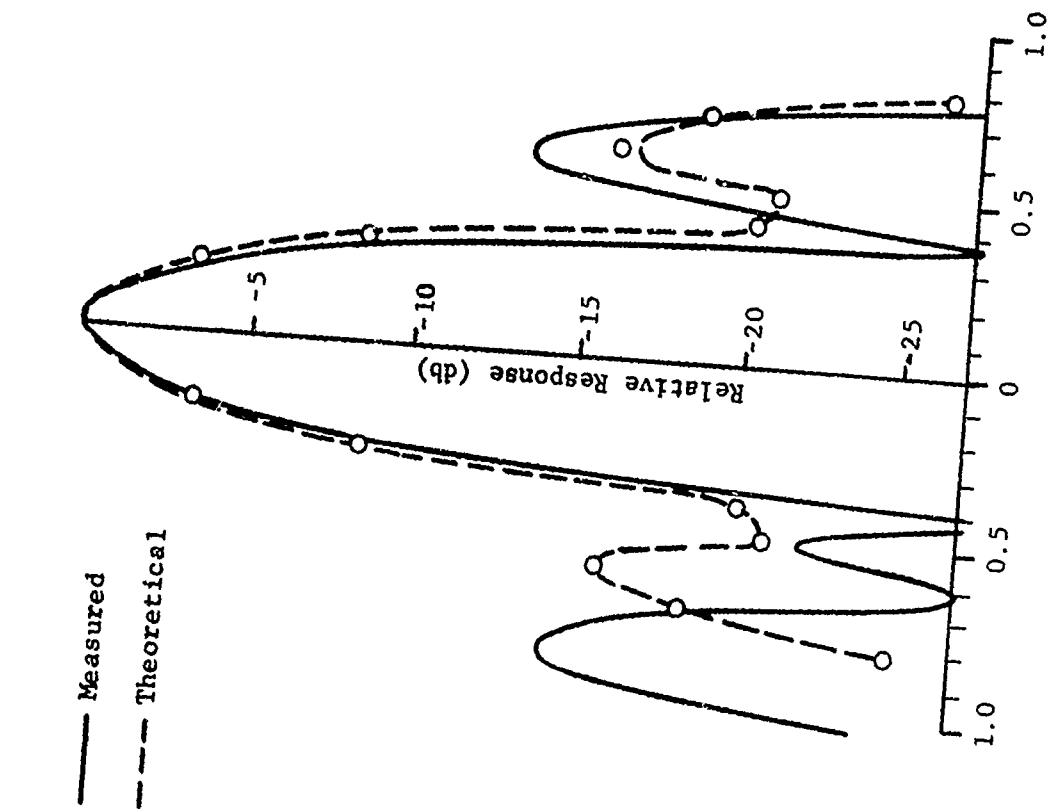


FIGURE 34. THEORETICAL AND MEASURED ON-AXIS DIRECTIONAL
RESPONSE AT 1 MHz (POLYSTYRENE LENS)

Polyethylene-Silicone Rubber Doublet Lens

The design parameters are shown in Figure 35. A measured and theoretical directional response pattern at 600 kHz is shown in Figure 36.

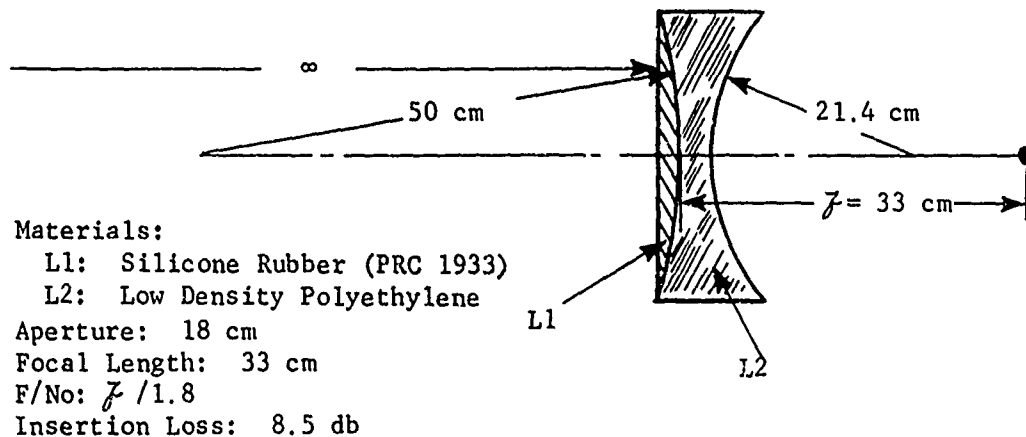


FIGURE 35. POLYETHYLENE AND SILICONE RUBBER
DOUBLET LENS PARAMETERS

Nylon-Silicone Rubber Doublet Lens

The design parameters are shown in Figure 37. The measured and theoretical directional response patterns at 600 kHz are shown in Figure 38.

Polyphenylene Oxide-Silicone Rubber Doublet Lens

Employing lens design Equations (21) through (26), a thermally corrected doublet was designed using polyphenylene oxide and silicone rubber (PRC-1933). The design parameters are shown in Figure 39. The focal length was selected to be 60 cm and the clear aperture 33 cm, yielding a $f/1.8$ lens.

(Text Continued on Page 58)

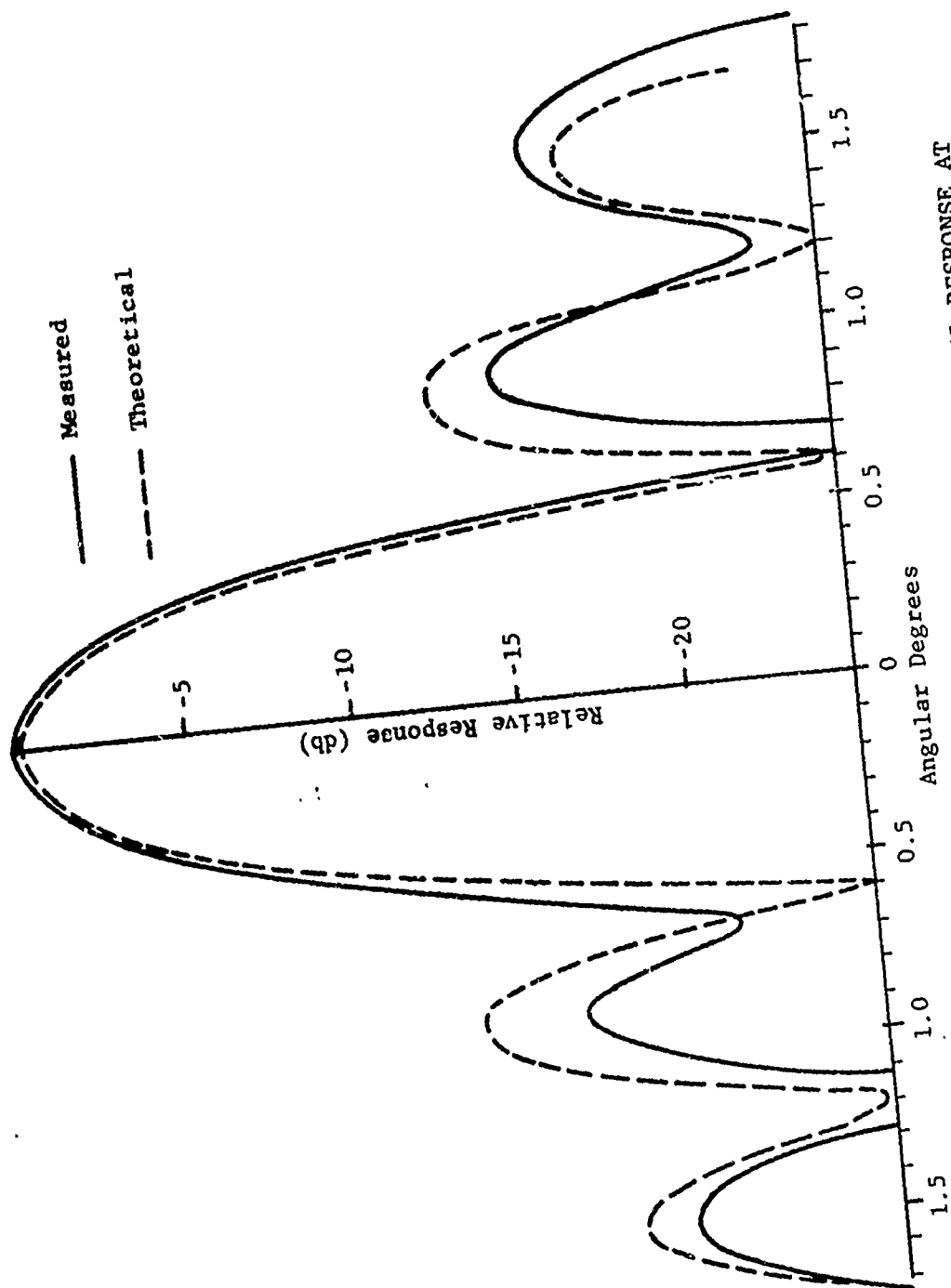


FIGURE 36. THEORETICAL AND MEASURED ON-AXIS DIRECTIONAL RESPONSE AT 600 kHz (POLYETHYLENE/SILICONE RUBBER LENS)

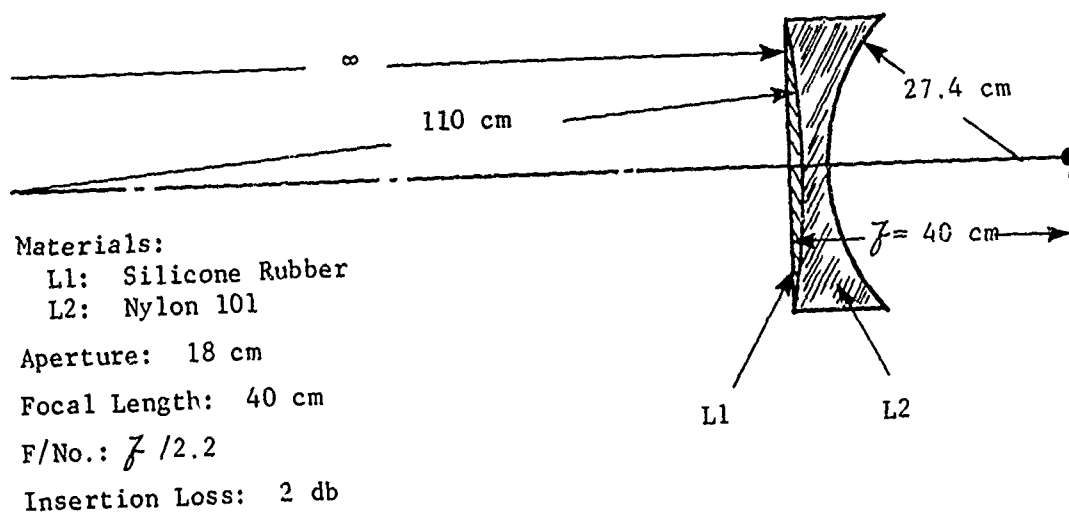


FIGURE 37. NYLON AND SILICONE RUBBER DOUBLET LENS PARAMETERS

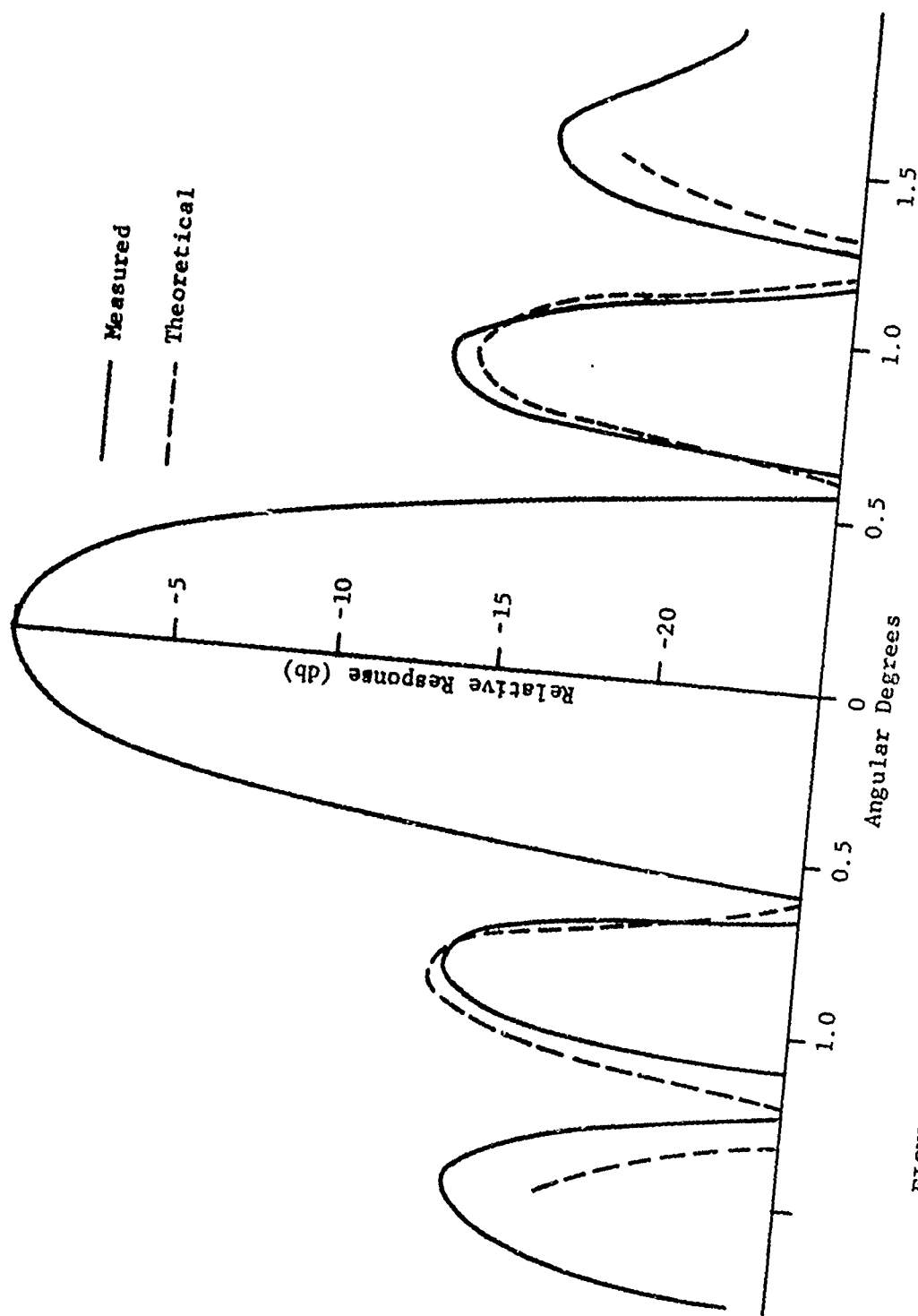


FIGURE 38. THEORETICAL AND MEASURED ON-AXIS DIRECTIONAL RESPONSE AT 600 kHz (NYLON/SILICONE RUBBER LENS)

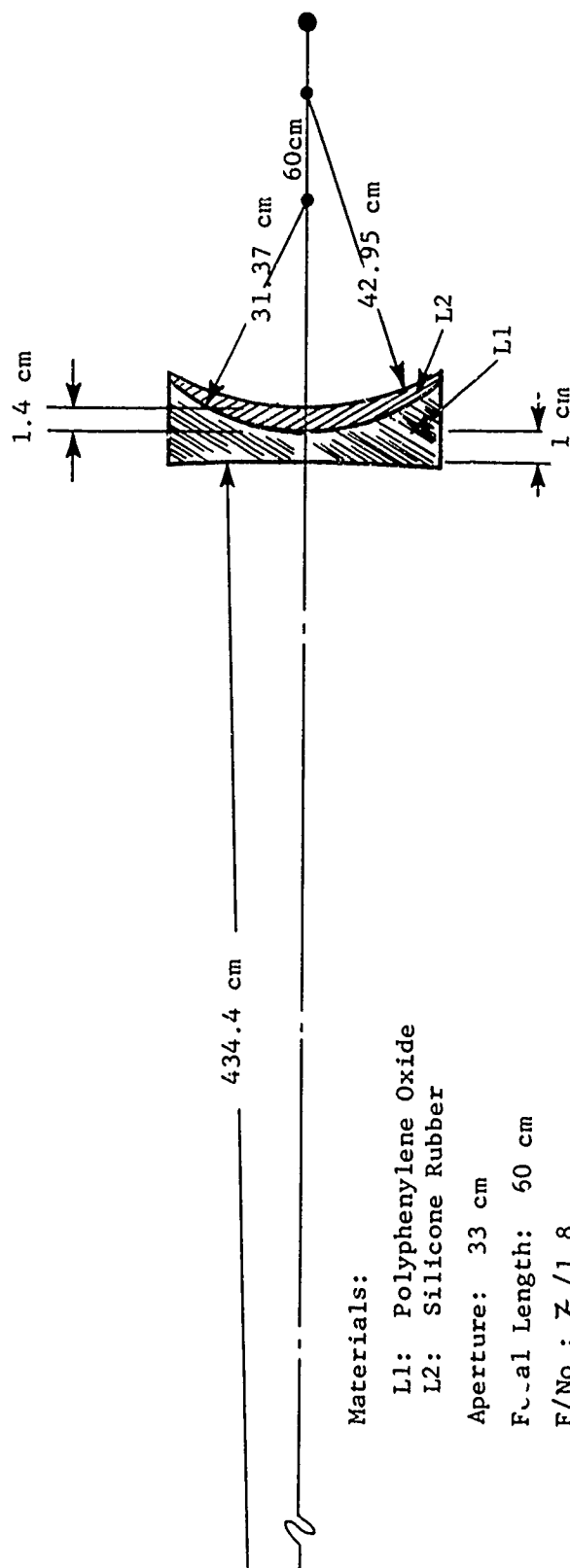


FIGURE 39. POLYPHENYLENE OXIDE AND SILICONE RUBBER
DOUBLET LENS PARAMETERS

Figure 40 shows the measured and theoretical on-axis directional response. Figure 41 shows the 20 degree off-axis directional responses as measured with a 0.5-cm wide transducer probe. The beamwidth for both cases is near 0.4 degree.

TEST RESULTS FOR MULTI-ELEMENT LENS SYSTEM

To investigate the feasibility of employing multi-element lens systems, the 4-element system shown in Figure 42 was tested.

Figure 43 shows the measured and theoretical directional responses at 600 kHz.

DISCUSSION OF TEST RESULTS

The results obtained for all lenses tested was uniformly good at 600 kHz. The directional responses were well formed and occurred at the proper position along the acoustic axis (within experimental error). Shading, which is a desirable characteristic in most applications, occurred in most cases as a result of the higher losses incurred at the aperture extremes due to the geometric shape of the lens (thin in middle, thick on edges).

Some degradation in directional responses was observed at a frequency of 1.2 MHz for the bi-concave polyethylene lens. The theoretical sidelobe level was considerably lower than the actual level. The polyethylene lens had a much rougher surface than the other lenses and the aberrations introduced at short wavelengths due to the surface roughness could account for the higher sidelobes. Since good results were obtained at frequencies above 1 MHz for the nylon and polystyrene lenses, the high sidelobes of the polyethylene lens probably do not represent any fundamental limitation.

The other case of serious departure from the theoretical and expected performance was observed for the polyphenylene oxide and silicone rubber doublet at 600 kHz. Again, higher sidelobes than expected were measured. The construction of this lens required the mixing of two component materials for the silicone rubber, evacuation in a vacuum, and heat curing for 24 hours. The large volume of silicone rubber required the mixing of several separate containers of material. Variations in sound velocity from one mix to another could account for the aberrations observed.

(Text Continued on Page 61)

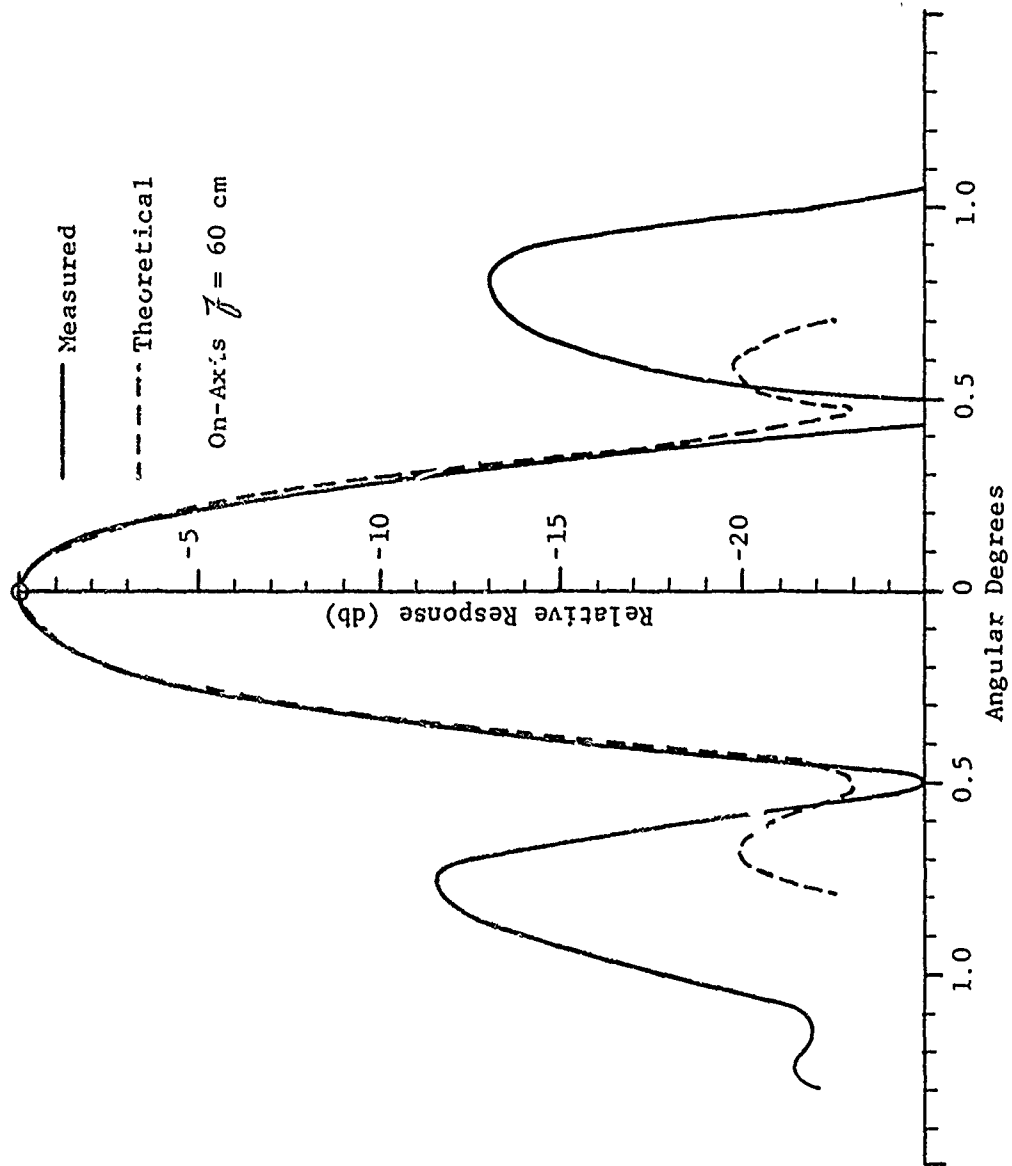


FIGURE 40. THEORETICAL AND MEASURED ON-AXIS DIRECTIONAL RESPONSE AT 600 kHz (POLYPHENYLENE OXIDE/SILICONE RUBBER LENS)

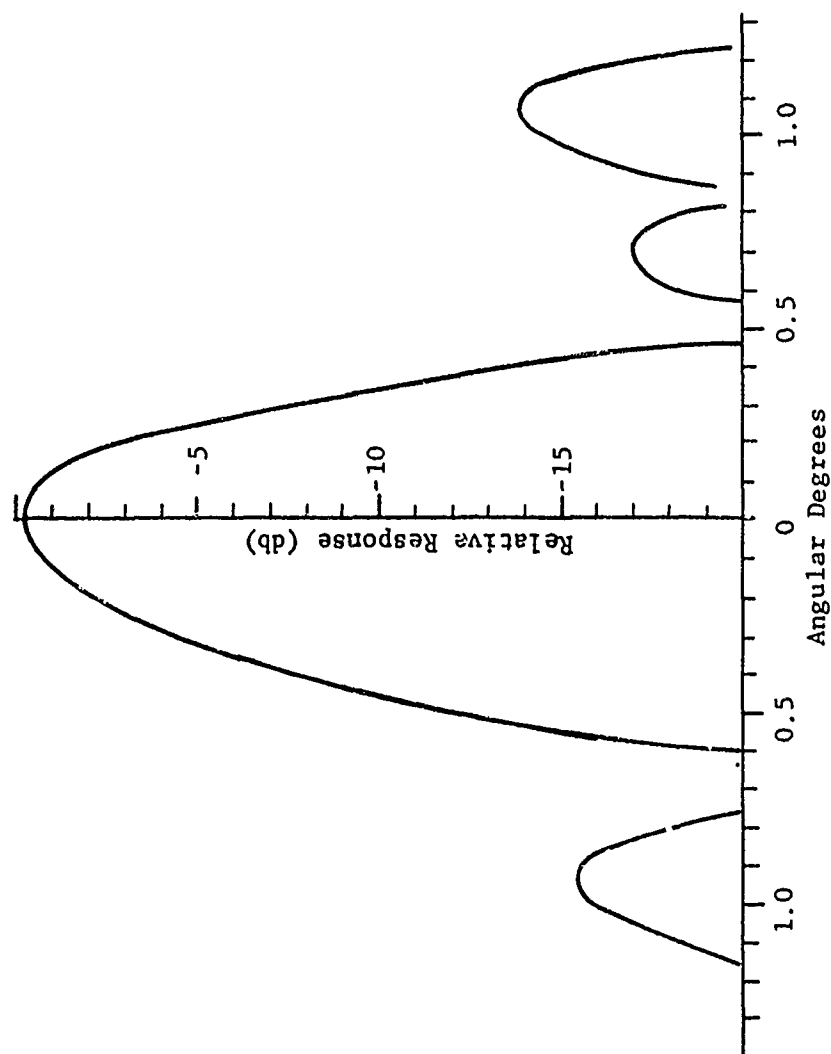
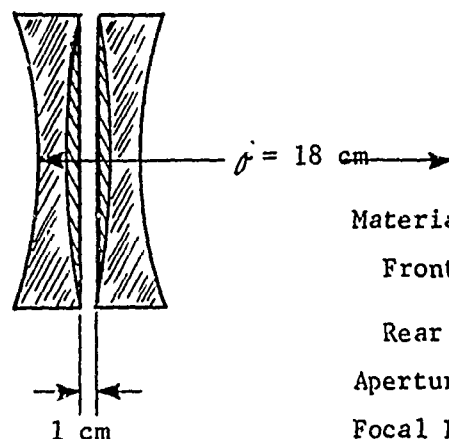


FIGURE 41. MEASURED DIRECTIONAL RESPONSE AT 600 kHz (POLYPHENYLENE OXIDE/SILICONE RUBBER LENS, 20° OFF-AXIS)



Materials:

Front Element: Polyethylene/Silicone Rubber

Rear Element: Nylon/Silicone Rubber

Aperture: 18 cm

Focal Length: 18 cm

F/No.: $f/1.0$

Insertion Loss: 9 db

FIGURE 42. MULTI-ELEMENT LENS PARAMETERS

CONCLUSIONS

The experimental data confirm both the thin lens optical design techniques and the theoretical lens analysis presented in Appendix B.

The singlet lens data show that good lens performance can be expected of low-, intermediate-, or high-absorption loss plastics. The results show that beamwidths in the order of 0.35 degrees over a 30 degree field of view can be obtained. Insertion losses in the order of 2 db as obtained with the nylon and polystyrene lenses at 600 kHz should not be prohibitively high for most applications. Though no syntactic foam material was available for lens fabrication during this work, it should not be ignored as a useful material. It should rank with polystyrene in terms of insertion loss and has the additional advantage of a good impedance match to seawater and a lower index of refraction.

An additional useful feature of the solid lens is its insensitivity to temperature variations. Also, due to the very small sound velocity

(Text Continued on Page 63)

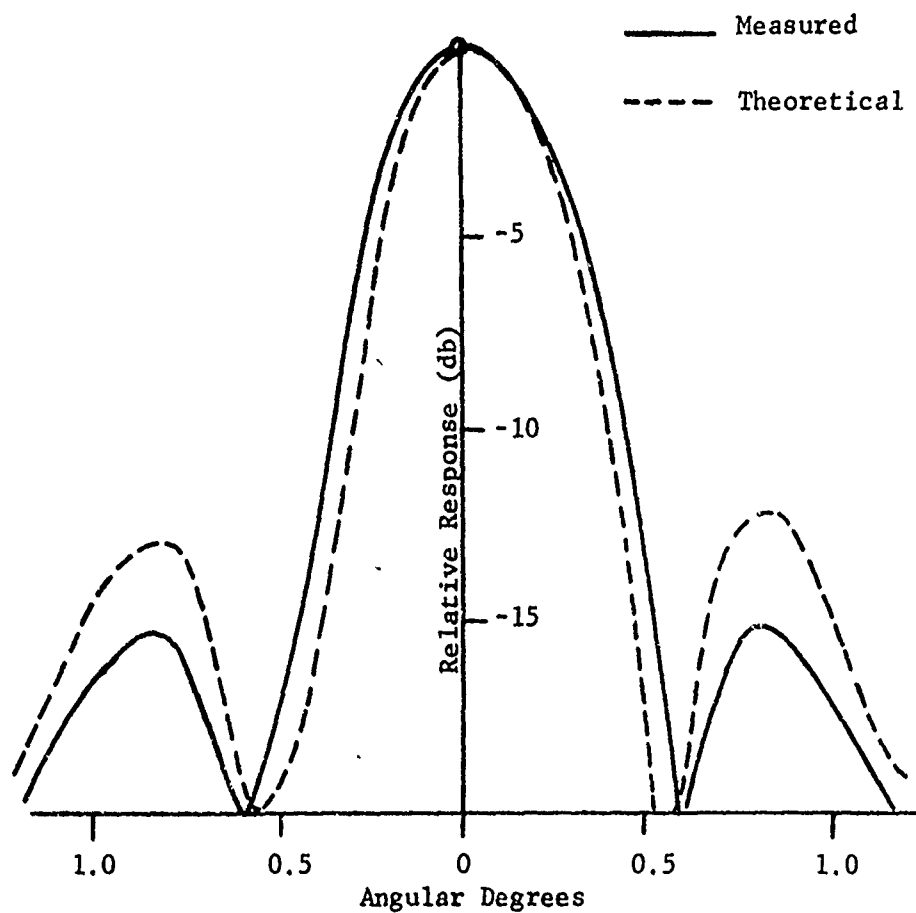


FIGURE 43. THEORETICAL AND MEASURED ON-AXIS DIRECTIONAL RESPONSE AT 600 kHz (MULTI-ELEMENT LENS)

variation as a function of pressure, it should be possible to operate over a depth range of several thousand feet with no significant changes in lens performance or focal length.

The doublet lens data demonstrate the feasibility of this type lens if the application warrants the additional aberration corrections. Obviously, however, a higher insertion loss will be encountered. It is apparent from these data that no significant degradation in performance is imposed by the solid-solid interface. It is probable that most applications of the solid lens technology will be satisfied by the singlet lenses. However, for applications requiring wider temperature ranges, wider fields of view, or other features requiring great amounts of aberration correction, the feasibility of the doublet lens has been established.

The multi-element lens system was tested to determine how far the optical lens design techniques could be pursued. It is apparent from the test data that a lens system of this type is feasible, but it is probable that multi-elements would not be required in the near future. However, the lens technology is available if system applications require a high performance lens of this type.

REFERENCES

1. Toulis, W. J., *Acoustic Focusing with Spherical Structures*, Journal of Acoustical Society of America, Vol. 35, pp. 286-292, March 1963.
2. Boyles, C. A., *Theory of Focusing Plane Waves by Spherical Liquid Lenses*, Journal Acoustical Society of America, Vol. 38, pp. 393-405, September 1965.
3. Folds, D. L., and Brown, D. H., *Focusing Properties of Cylindrical Liquid-Filled Acoustic Lenses with Large Diameter-to-Wavelength Ratios*, Journal of Acoustical Society of America, Vol. 43, No. 3, pp. 560-565, March 1968.
4. Naval Ship Research and Development Laboratory Report 2738 (Revised), *Considerations in the Design of Cylindrical Liquid-Filled Acoustic Lenses*, by D. L. Folds, March 1969.
5. Folds, D. L., *Focusing Properties of a Cylindrical Liquid-Filled Compound Acoustic Lens*, Journal of Acoustical Society of America, Vol. 49 (Part 2) pp. 1591-1595, May 1971.
6. Carswell, A. I., and Richard, C., *Focal Properties of Microwave Lenses with Small F-Numbers*, Applied Optics, Vol. 10, pp. 346-357, February 1971.
7. Jenkins, F. A., and White, H. E., *Fundamentals of Optics*, McGraw Hill Book Company, New York (1957).
8. Smith, W. J., *Modern Optical Engineering*, p. 401, McGraw Hill Book Company, New York (1966).
9. Conrady, A. E., *Applied Optics and Optical Design, Part I*, p. 289, Dover Publications, Inc., New York (1957).
10. Pennwalt Corporation Final Report Contract N61339-69-C-0011, *Fluids for Acoustic Lenses*, by G. R. Leader, A. H. Fainberg, R. L. Atwell, and J. R. Soulen, August 1969.

APPENDIX A

LENS CONSTRUCTION MATERIALS

SOLIDS

The acoustic properties of a number of plastic materials have been measured using a time of travel technique. Samples of these materials having dimensions of approximately 5 (± 0.01) cm on a side were clamped between a transmitting transducer and a receiving transducer (frequency = 500 kHz). The time delay of a 20-microsecond pulse was measured to an accuracy of ± 0.02 microsecond and converted to a sound velocity in m/sec. This measurement was repeated at several temperatures in the range 0 to 30°C, while the sample and transducer were immersed in a constant temperature bath. Temperature was held constant within $\pm 0.2^\circ\text{C}$ as measured with digital thermometer probes in the bath.

The accuracy for all sound velocity measurements was well within ± 8 m/sec limits. The rms error in fitting the data to straight lines for sound velocity versus temperature was less than 3 m/sec for all but two of the samples tested. Table A1 lists the measured data for the solid materials. The list is arranged according to sound velocity value at 0°C. Also listed are indices of refraction at 20°C for salinities of 0 and 30 ppm, dn/dt for these salinity values and density. Figure A1 graphs the position of each material according to its acoustic impedance. Note that most of the materials lie between the $\rho V = 2.0$ and $\rho V = 2.5$ contours on the graph. Syntactic foam and PRC 1933-2 silicone rubber materials have impedance values near that of water, and are also at opposite extremes in sound velocity.

An interesting relationship between dV/dt and transmission loss was observed for this group of materials. This is shown in Figure A2 where dV/dt is the left ordinate, and measured transmission loss through the 5-cm sample immersed in water at a frequency of 500 kHz is the right ordinate.

The transmission loss through a small sample is not a precise measure of attenuation for a material, but for materials of similar acoustic impedance values and high attenuations, it can be a good relative measure of attenuation. Transmission loss through 10-cm thick slabs of nylon, syntactic foam (41#/ft³), polystyrene, and polyethylene ($\rho = 0.93$) g/cc was measured as a function of frequency. These data are plotted in Figure A3 as attenuation in db/cm.

Table A2 lists information concerning material source and description.

(Text Continued on Page A-7)

TABLE A1
ACOUSTIC PROPERTIES OF SOLID MATERIALS

Material	Velocity, 0°C m/sec	dv/dt m/sec°C	RMS Error m/sec	n, 20°C Salinity = 0 ppm	n, 20°C Salinity = 30 ppm	dn/dt x 10 ³ Salinity = 0 ppm	γ	ρ gm/cc
Polypropylene	2792	-9.55	2.99	0.570	0.583	3.40	-4.2	0.90
Acrylic	2717	-2.1	-	0.554	0.567	1.92	-7.7	1.29
Nylon 101 (1)	2712	-3.15	2.06	0.559	0.572	2.1	-7.0	1.15
Nylon 101 (2)	2705	-3.45	2.81	0.563	0.575	2.2	-6.6	1.15
Penton	2569	-5.70	2.68	0.604	0.618	2.9	-4.5	1.40
Linear P/E	2559	-5.97	3.10	0.608	0.621	3.0	-4.3	0.95
Delux D	2515	-6.97	2.86	0.624	0.638	3.3	-3.8	1.42
Celcon	2513	-6.35	0.98	0.622	0.635	3.2	-3.9	1.41
Synthetic Foam	2585	-1.21	2.69	0.579	0.592	1.8	-7.8	0.57
UHMW P/E	2364	-5.44	3.11	0.658	0.672	3.2	-3.5	0.93
Polystyrene	2334	-1.17	1.14	0.642	0.656	2.0	-5.9	1.04
PSO	2297	-1.38	-	0.656	0.670	2.2	-5.2	1.24
NORYL	2296	-1.70	4.00	0.655	0.670	2.2	-5.2	1.08
PFO	2293	-1.52	1.65	0.655	0.670	2.2	-5.2	1.09
LEXAN	2280	-3.58	2.39	0.671	0.686	2.8	-3.9	1.19
CYCOLAC	2268	-2.70	1.32	0.669	0.685	2.6	-4.2	1.12
Natural P/E	2266	-8.69	1.83	0.709	0.725	4.5	-2.1	0.94
Hi-Impact Polystyrene	2242	-3.26	0.90	0.681	0.696	2.8	-3.8	1.03
PRC-1933-2	948	-2.47	1.46	1.65	1.68	8.5	+2.5	1.48
3-M Fluoroelastomer	872	-2.61	0.75	1.81	1.85	10.0	+2.7	-
Low Density P/E	2280	-8.77	2.99	0.705	0.720	4.4	-2.2	0.93

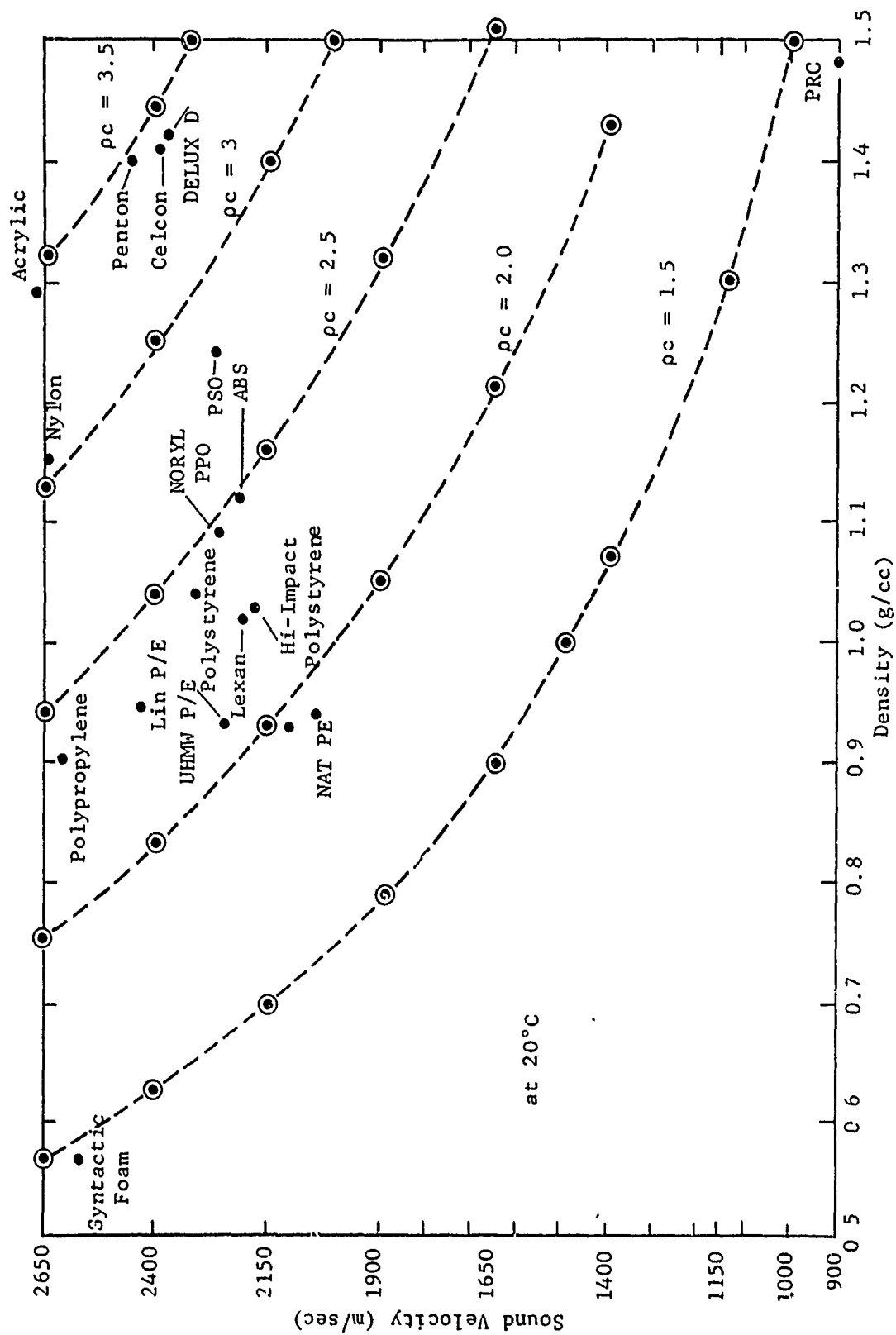


FIGURE A1. SOUND VELOCITY VERSUS DENSITY FOR SOLID MATERIALS

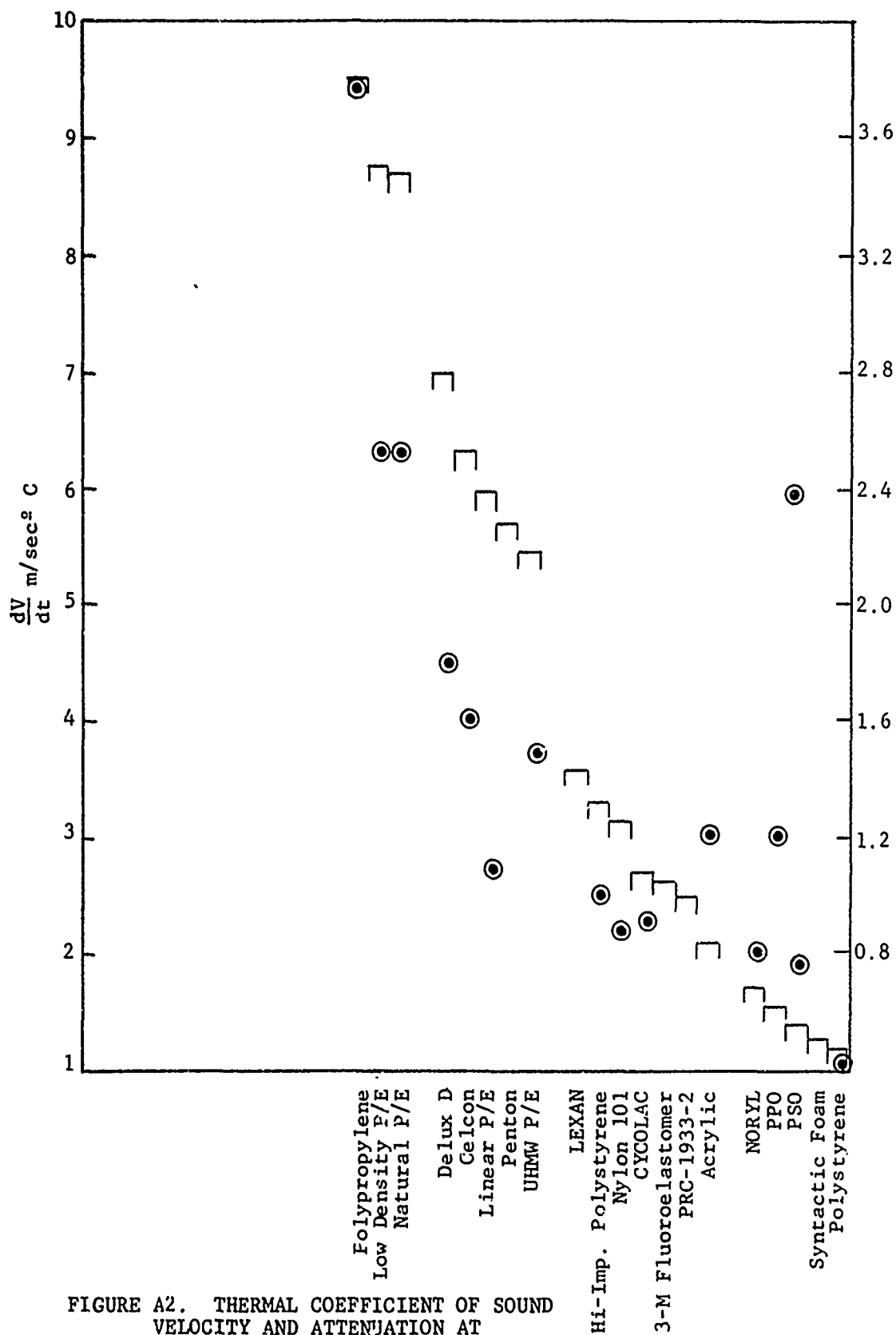


FIGURE A2. THERMAL COEFFICIENT OF SOUND VELOCITY AND ATTENUATION AT 500 kHz FOR SOLID MATERIALS

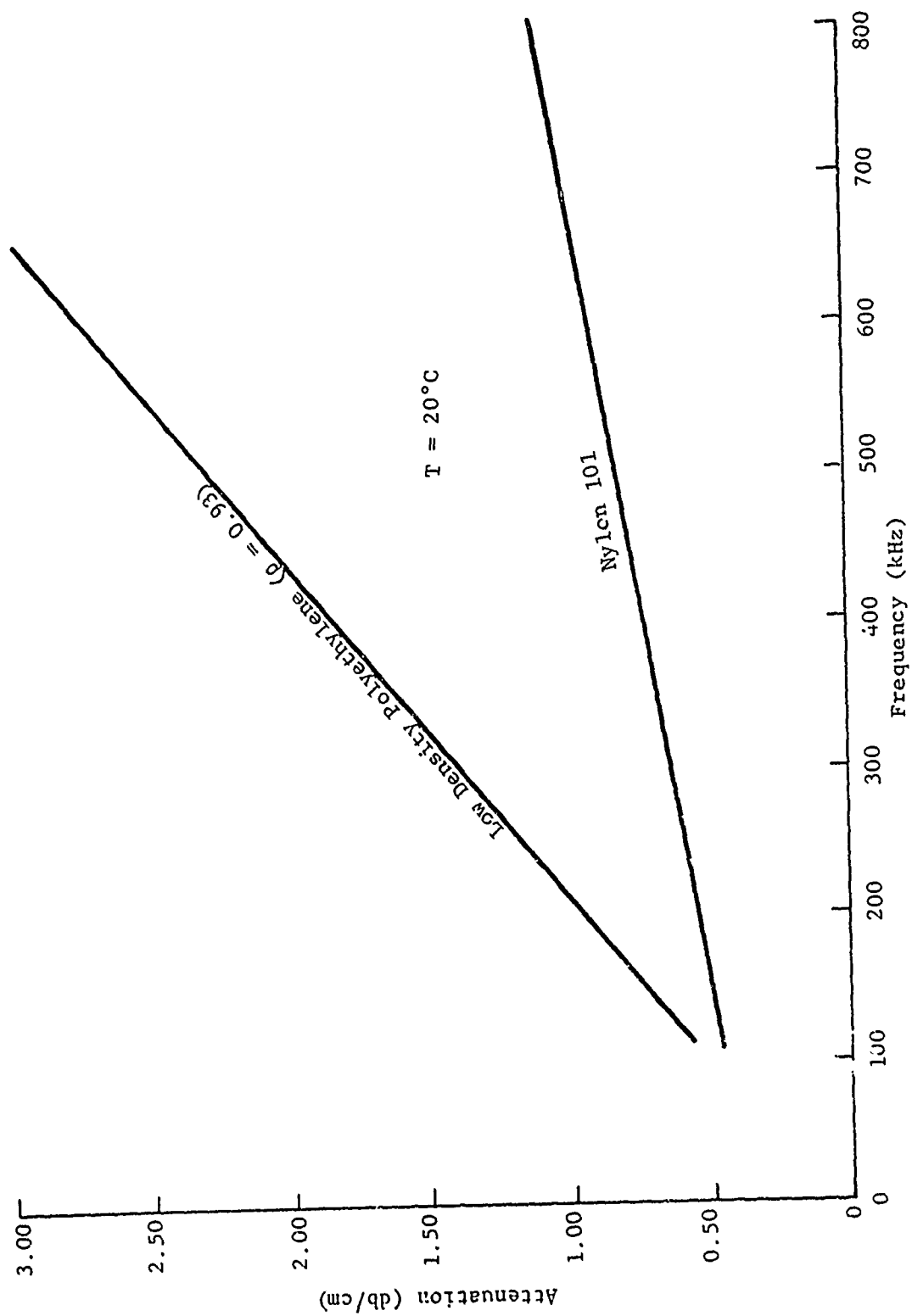


FIGURE A3. ATTENUATION AS A FUNCTION OF FREQUENCY FOR NYLON AND POLYETHYLENE

TABLE A2
SOLID MATERIAL SOURCE AND DESCRIPTION

<u>Formula Trade Name</u>	<u>Generic Name</u>	<u>Manufacturer</u>
CYCOLAC	Acrylic Butadiene Styrene (ABS)	Merbon Chemical Co.
Hi-Impact Polystyrene (Styron)	Modified Polystyrene	Dow Chemical Co.
Plexiglass, Acrylic, Lucite	Crystal Methacrylate	Rohm & Hass DuPont
PPO	Polyphenylene Oxide	General Electric
CELCON	Acetal Copolymer	Celanese Corp.
Delrin (Delux-D)	Acetal Homopolymer	DuPont
Delrin AF	Acetal and Teflon Resin	DuPont
DFD 0600 Natural Polyethylene	Low Density Polyethylene	Union Carbide
Marlex 5003 Linear Polyethylene	High Density Polyethylene	Phillips Chemical Co.
Hi-Fax 1900 UHMW	Ultra High Molecular Weight Polyethylene	Hercules, Inc.
PROFAX	Polypropylene	Hercules, Inc.
ZYTEL 101	Nylon	DuPont
NORYL	Modified Phenylene Oxide	General Electric
PENTON	Chlorinated Polether	Hercules, Inc.
Styrene 50-D	Crystal Polystyrene	Foster Grant
PSO	Polysulfone Resin	Union Carbide
LEXAN	Polycarbonate	General Electric
WR-107-1	Syntactic Foam	3M Co.
WR-106-1	Fluoroelastomer	3M Co.
PRC 1933-2	Silicone Rubber	Products Research Co.

LIQUIDS

The acoustic properties of a large number of liquids have been measured and tabulated in References A1, A2, and A3. Those liquids which have been found useful in liquid lenses are listed in Table A3.

All of the FC and FS series liquids are inert and compatible with almost all lens construction materials.

It is interesting to compare dV/dt for the liquid and solid materials. The liquids are all in the range -2.5 to -4 m/sec-°C while the solids range from -1 to -9 m/sec-°C.

REFERENCES

- A1. Pennwalt Corporation Final Report Contract N61339-69-C-0011, *Fluids for Acoustic Lenses*, by G. R. Leader, A. H. Fainberg, R. L. Atwell, and J. R. Soulen, August 1969.
- A2. Schaffs, W., *Numerical Data and Functional Relationships in Science and Technology, Group II: Atomic and Molecular Physics, Vol. 5, Molecular Acoustics*, Springer-Verlag, New York, 1967.
- A3. U.S. Naval Electronics Laboratory TM-437, *Table of Compiled Experimental Values of the Physical and Ultrasonic Properties of Over 200 Liquids*, by E. W. Rusche and R. W. Prather, November 1960.

APPENDIX B

NUMERICAL CALCULATION OF PRESSURE DISTRIBUTION IN IMAGE SPACE

Although the geometric theory of thin lens design is a powerful tool and will provide a good first approximation lens design, other methods are required to give precise lens performance data. The most important characteristic of the lens is its diffraction pattern or, in sonar terms, directional response. Therefore, the computation of directional response for given lens parameters forms an important part of lens analysis.

The computation of the directional response is accomplished by numerical calculation of the pressure distribution in image space by solving the Fresnel-Kirchoff diffraction formula. The Fresnel-Kirchoff relationship written in terms of two-dimensional lens parameters is

$$U(x_i, z_i) = C \int_{-d/2}^{d/2} A(r) e^{-ikr} dx$$

where parameters of Figure B1 are used. The y-dimension is suppressed.

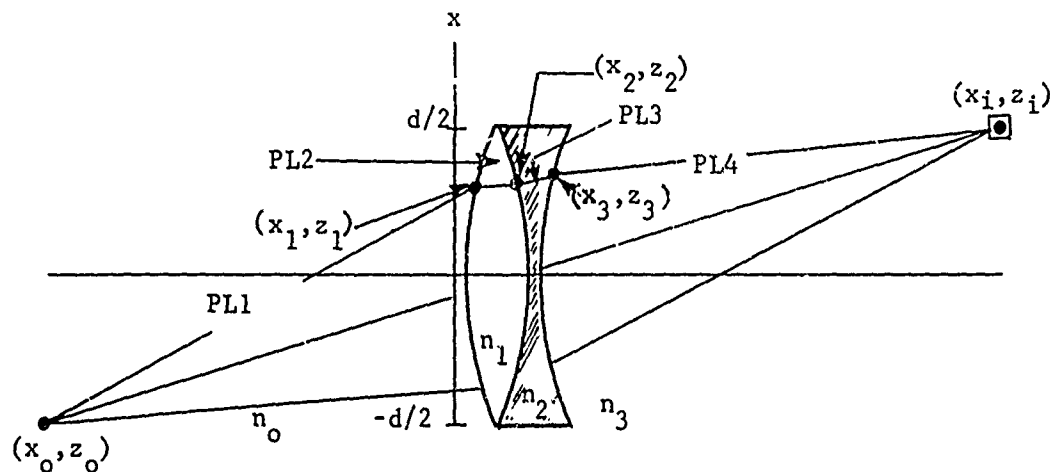


FIGURE B1. GEOMETRY USED FOR NUMERICAL CALCULATION
OF PRESSURE DISTRIBUTIONS IN IMAGE SPACE

In this form of the diffraction integral, $U(x_i, z_i)$ represents the complex pressure amplitude at a point in image space. The parameter r is the physical path length of an acoustic ray between the points x_0, z_0 , and x_i, z_i . The parameter r is a function of x_0, z_0, x_i, z_i, x , the lens geometry, and refractive index (n). The function $A(r)$ is a complex amplitude weighting function which includes the absorption of the lens and the orientation of the acoustic sensor in image space. C is a complex constant introduced to absorb terms independent of x which only affect the magnitude and relative phase of the diffraction pattern and not its shape. The specific numerical calculations required to solve the diffraction integral are described below.

For a given x value between the limits $\pm d/2$, a ray path length, PL_1 , from the object to the lens first surface x_1, z_1 is calculated. Using Snell's law, $PL_2, PL_3, (x_2, z_2)$, and (x_3, z_3) are also calculated. The final path length PL_4 is calculated as geometric distance from (x_3, z_3) to (x_i, z_i) . The refraction angle is not calculated at the last surface because, for all cases of interest, the obliquity angle is small. To determine the complex amplitude weighting factor imposed by the sensor dimension and orientation, the geometry of Figure B2 is

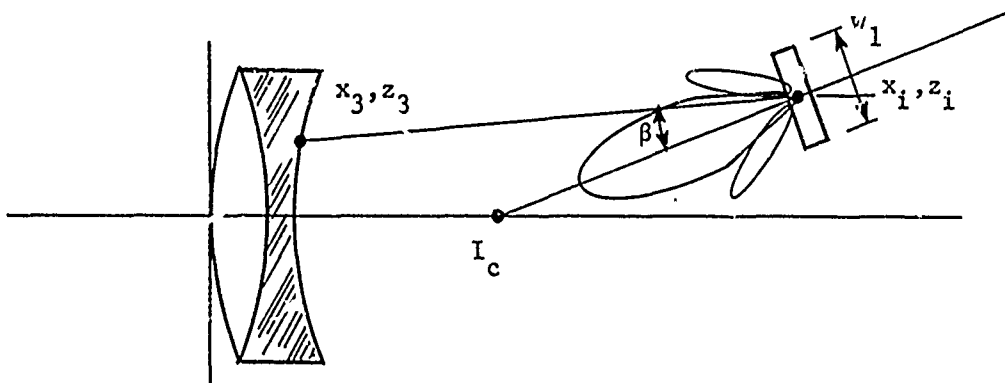


FIGURE B2. GEOMETRY FOR INCLUDING ELEMENT SIZE AND ORIENTATION IN CALCULATIONS

used. In this figure a $\sin(\pi u)/(\pi u)$ pattern, which represents the element directional response, is shown with the axis of maximum response perpendicular to the element and crossing the z-axis at I_c . The element width, w , and I_c are input parameters to the computer program. The complex weighting factor is then computed from the calculated angle β which is different for each incoming ray; i.e., $u = \sin(\beta) \cdot W_\lambda$, where W_λ is element width expressed in wavelengths.

The amplitude contribution A_j of a single ray, j , from (x_0, z_0) to (x_1, z_1) is given as

$$A_j = \left(\prod_k PL_k \cdot A_k \right) |\sin(\pi \cdot u_j)/(\pi \cdot u_j)|$$

where PL_k and A_k are path length and absorption through medium k .

The phase contribution of the same ray is given by

$$\phi_j = \frac{2\pi}{\lambda} \left[\sum_k PL_k \cdot n_k \right] + 0.5 \cdot \text{sign} \left[\sin(\pi u_j)/(\pi u_j) \right]$$

where the second factor accounts for the 180-degree phase shift observed in the odd-order sidelobes of the element diffraction pattern.

The magnitude of the pressure amplitude $A(x_1, z_1)$ at (x_1, z_1) is then given by

$$A(x_1, z_1) = \left[\left(\sum_j A_j \cos \phi_j \right)^2 + \left(\sum_j A_j \sin \phi_j \right)^2 \right]^{1/2}.$$